

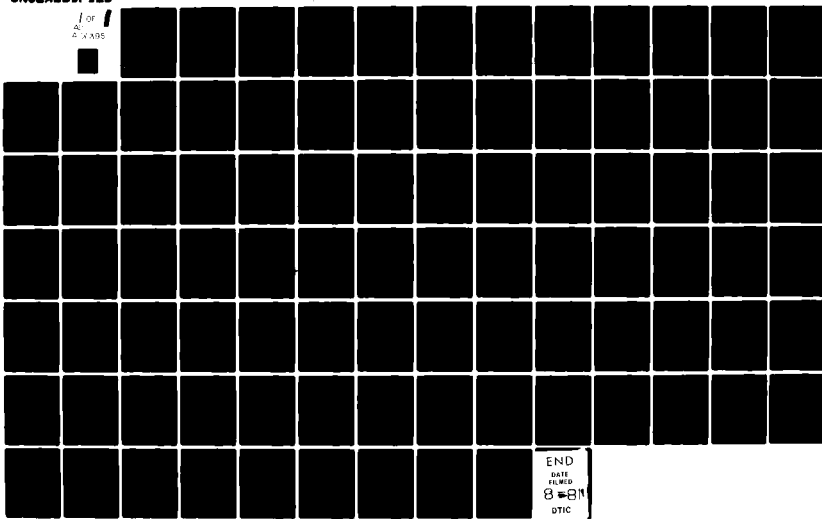
AD-A101 395

SOIL CONSERVATION SERVICE OXFORD MS SEDIMENTATION LAB F/8 8/8  
STREAM CHANNEL STABILITY. APPENDIX J. NUMERICAL MODEL FOR ROUTE—ETC(U)  
APR 81 C V ALONSO, D K BORAH, S N PRASAD

UNCLASSIFIED

NL

for  
AC  
6 XA95



END  
DATE  
FILED  
8-8-81  
DTIC

✓  
LFVEL ~~II~~  
AD A101395

(1)

## STREAM CHANNEL STABILITY

APPENDIX J

### NUMERICAL MODEL FOR ROUTING GRADED SEDIMENTS IN ALLUVIAL CHANNELS

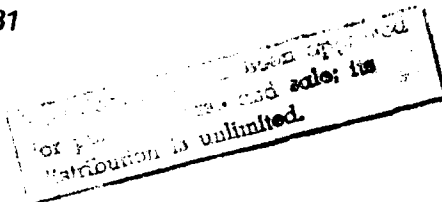
*Project Objective 4*

*by*

C. V. Alonso, D. K. Borah  
and S. N. Prasad

USDA Sedimentation Laboratory  
Oxford, Mississippi

April 1981



Prepared for  
US Army Corps of Engineers, Vicksburg District  
Vicksburg, Mississippi

Under  
Section 32 Program, Work Unit 7

DTIC FILE COPY

81 7 14 097

STREAM CHANNEL STABILITY.

APPENDIX J

NUMERICAL MODEL FOR ROUTING  
GRADED SEDIMENTS IN ALLUVIAL CHANNELS

Project Objective 4

by

15 Carlos V. Alonso<sup>1/</sup>, Deva K. Borah<sup>2/</sup> and S. N. Prasad<sup>3/</sup>

USDA Sedimentation Laboratory

Oxford, Mississippi

11 April 1981

12 94

Prepared for

US Army Corps of Engineers, Vicksburg District  
Vicksburg, Mississippi

Under

Section 32 Program, Work Unit 7

- 1/ Research Hydraulic Engineer, Sediment Transport and Deposition Research Unit, USDA Sedimentation Laboratory, Oxford, MS.
- 2/ Research Associate, Department of Civil Engineering, The University of Mississippi, University, MS.
- 3/ Professor, Department of Civil Engineering, The University of Mississippi, University, MS.

11-461

## PREFACE

The main objective of this study is to develop a numerical model for simulating the movement of well graded sediment through a stream network. In Part 2 of this report the theoretical background of the model is described and the governing equations are formulated. The numerical solution of these equations is presented in Part 3. Hydraulic routing can be performed using any acceptable algorithm supplied by the user because the water movement is assumed to be uncoupled from the sediment process. The model can be used in conjunction with any suitable sediment yield model to supply the water and sediment runoff from lateral areas. The application and results of the model are discussed in Part 4. The computer program for the numerical model of the East Fork River system is described and listed in the third addendum.

Accession For	
NTIS GRA&I	
DTIC TAB	
Unclassified	
Distribution	
Per Form 50	
By <i>on file</i>	
Distribution	
Availability Codes	
Dist	Avail under Special
A	

## TABLE OF CONTENTS

List of Tables .....	3
List of Figures .....	4
U.S. Customary to S.I.-Units Conversion Factors .....	5
1.    Introduction .....	6
2.    Model Formulation .....	8
2.1    Equations of Motion .....	8
2.2    Ancillary Algorithms .....	15
2.2.1    Sediment Transport Formulas .....	15
2.2.2    Residual Capacity. Composition of Material in Transport .....	16
2.2.3    Bed Composition ....	17
2.2.4    Bed Erosion. Armoring .....	25
2.2.5    Sediment Deposition .....	29
3    Numerical Scheme .....	32
4    Model Testing .....	36
4.1    Flume Armoring Study .....	37
4.2    San Luis Valley Canal Tests .....	40
4.3    East Fork River Project .....	42
5    Conclusions and Recommendations .....	52
5.1    Conclusions .....	52
5.2    Recommendations .....	52
References .....	54
Addendum 1. Sediment Continuity Equation .....	57
Addendum 2. Summary of Transport Formulas .....	63
Addendum 3. Description of Computer Program .....	65

## LIST OF TABLES

### Table

1. Hydraulic conditions in the flume and San Luis Valley Canal studies .....	38
2. Size distributions used for simulating the flume and San Luis Valley Canal data .....	38

## LIST OF FIGURES

### **Figure**

1. Definition sketch .....	9
2. Routing of water and sediment characteristic waves .....	14
3. Schematic representation of bed processes .....	18
4. Schematic representation of active layer composition .....	21
5. Graphical representation of $y$ -matrix components .....	23
6. Erosion loop .....	27
7. Adjustment of active-layer thickness .....	28
8. Deposition loop .....	31
9. Grid used in sediment characteristic solution .....	33
10. Load upgrading loop .....	33
11. Organization of numerical scheme .....	34
12. Size distribution curves obtained for flume armoring test .....	39
13. Evolution of the size distribution in top layer of San Luis Valley Canal .....	41
14. East Fork River study reach .....	43
15. Examples of reach cross sections .....	45
16. Flow and sediment rating curves .....	46
17. Measured and predicted flows at station B-17, East Fork River ...	48
18. Measured and predicted bedloads at station B-17, East Fork River	49
19. Measured and predicted bedload size-distributions at station B-17, East Fork River .....	51
1.1 Definition sketch of vertical transfer .....	58

U.S. Customary to S.I.-Units Conversion Factors

To convert	To	Multiply by
inches (in.)	millimeters (mm)	25.4
feet (ft)	meters (m)	0.305
yards (yd)	meters (m)	0.914
miles (miles)	kilometers (km)	1.61
square inches (sq. in.)	square millimeters ( $\text{mm}^2$ )	645
square feet (sq ft)	square meters ( $\text{m}^2$ )	0.093
square yards (sq yd)	square meters ( $\text{m}^2$ )	0.836
square miles (sq miles)	square kilometers ( $\text{km}^2$ )	2.59
acres (acre)	hectares (ha)	0.405
cubic inches (cu in.)	cubic millimeters ( $\text{mm}^3$ )	16,400
cubic feet (cu ft)	cubic meters ( $\text{m}^3$ )	0.028
cubic yards (cu yd)	cubic meters ( $\text{m}^3$ )	0.765
pounds (lb) mass	kilograms (kg)	0.453
tons (ton) mass	kilograms (kg)	907
pound force (lbf)	newtons (N)	4.45
kilogram force (kgf)	newtons (N)	9.81
pounds per square foot (psf)	pascals (Pa)	47.9
pounds per square inch (psi)	kilopascals (kPa)	6.89
U.S. gallons (gal)	liters (L)	3.79
acre-feet (acre-ft)	cubic meters ( $\text{m}^3$ )	1,233

## INTRODUCTION

This report describes a one-dimensional numerical model designed to simulate sediment transport in natural channels. The physical processes associated with the sediment movement are reproduced using a variety of algorithms. These algorithms incorporate sets of equations that operate on input data in a predetermined sequence to generate output data reproducing the actual physical process. A satisfactory model must include the more relevant aspects of that process.

Sediment moves driven by hydrodynamic forces exerted by the flow of water which in many instances is highly time dependent. The sediment transport model must, therefore, account for unsteadiness in sediment movement.

The dependence of sediment motion on flow conditions makes it also dependent on the longitudinal variations the flow experiences as a result of stream boundary irregularities. These variations are reflected in the spatial variability of the sediment load distribution. Depending on particle size, some particles may be carried primarily in suspension, while others move entirely as bed load. In addition, depending on flow conditions, particles moving in suspension at one place may be moving as bed load farther downstream. Whether a particular size fraction moves primarily as suspended load or bed load determines to what extent that fraction of the sediment load will lag behind the flood wave and therefore determines what the magnitude of longitudinal sorting will be. This means that the transport model must reflect the dependence of the sediment load lag on the material properties of the sediment as well as on hydraulic conditions. Whenever the bed material consists of a mixture, its transport involves the motion of a multitude of particles of diverse sizes. Some particles may deposit on the streambed while others are scoured away, resulting in a size composition of the material in transport different from that of the bed. A realistic model must account for the interchange between the bed surface material and the moving sediment load, and should simulate the residual transport capacity of the stream. The latter is a measure of the ability of the flow to further entrain material of a given size fraction in the presence of all the fractions already in motion.

During the above particle interchange, the bed material particle size composition changes continuously and, in the process, the bed may experience a net amount of aggradation or degradation. For certain flow conditions the bed degradation in a reach may be limited by the formation of an armoring layer, over which sediment may move either in suspension or as intermittent bed-load waves. The armoring layer may be destroyed during high flows and reformed at subsequent low flows. A model must therefore be capable of tracking the streambed profile evolution and the changes in bed material size distribution.

The proposed model is designed to meet the above criteria. It can simulate the unsteady transport of sediment mixtures through a network of nonbifurcating channel reaches, and it can be used in tandem with a suitable sediment yield model, like the one described by Borah et al. (1981), which simulates the supply of water and sediment runoff from adjacent upland areas. At present the model is restricted to consideration of noncohesive bed materials only. It is also restricted to down channel streamflow, and cannot consider the effect of transverse currents.

Parts 2 and 3 of this report provide a detailed description of the model. Part 4 discusses the validation of the model on sets of laboratory and field data. Coding details are given in Addendum 3. Some of this material has been presented in an earlier report (Borah, 1979).

## MODEL FORMULATION

## 2.1 EQUATIONS OF MOTION

The present model treats the time-dependent problem of one-dimensional sediment routing in alluvial channels. The hydraulic functions driving the sediment movement are the local flow discharge, stage, and cross-sectional flow area. Therefore, an unsteady flow algorithm is required to compute the time and space distribution of those flow parameters in the channel, given information concerning channel geometry, history of inflowing water discharge, and/or downstream stage.

One-dimensional hydraulic routing algorithms are usually based on the shallow-water equations of momentum and conservation of mass for sediment-laden water. In natural streams load concentrations of up to 50,000 ppm will not change the density of the mixture by more than 3%. Thus, density variations may be ignored. Furthermore, within that range of concentrations, the surface waves propagate with a velocity that is practically unaffected by the erodibility of the bed (Gradowczyk, 1968). The governing equations for water movement can thus be written

$$\frac{\partial Q}{\partial t} + \frac{\partial \beta QV}{\partial x} + gA \frac{\partial y}{\partial x} = \rho g A (S_o - S_f + \frac{q_w V_\ell}{Ag}), \quad (1)$$

$$\frac{\partial Q}{\partial x} + \frac{\partial A}{\partial t} = q_w, \quad (2)$$

where  $A$  is the flow cross-sectional area,  $g$  is the acceleration of gravity,  $Q$  is the flow discharge,  $q_w$  is the lateral water inflow per unit length of channel,  $S_o$  is the bed slope,  $S_f$  is the friction slope,  $t$  is time,  $V$  is the mean flow velocity,  $V_\ell$  is the velocity component of lateral inflow in the main flow direction,  $x$  is the horizontal distance along the channel,  $y$  is the flow depth,  $\beta$  is the momentum coefficient, and  $\rho$  is the water density (Fig. 1).

Two approximations to Eqs. 1 and 2 have found wide application in unsteady flow routing. They are the diffusion and kinematic wave approximations (Ponce, Li, and Simons, 1978). The first assumes that the inertia terms are negligible, while the second assumes that both the inertia and pressure terms can be neglected. Both approximations have been shown to be satisfactory in a variety of cases. Solutions of the

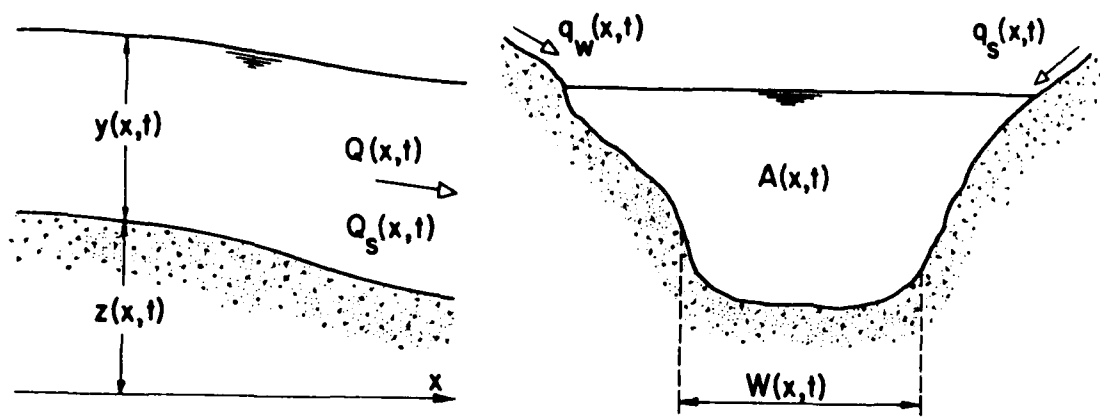


Fig. 1. Definition Sketch

complete shallow-water equations and their various approximations have been extensively discussed in the literature (Miller and Yevjevich, 1975) and they will not be considered in this paper. Any acceptable hydraulic algorithm will suffice since the water movement is assumed to be uncoupled from the sediment processes.

The third equation of motion is given by the conservation of mass equation for sediment. As shown in Addendum 1, this equation can be expressed in the form

$$\frac{\partial Ac}{\partial t} + \frac{\partial Q_s}{\partial x} + (1-\lambda)\lambda \frac{\partial z}{\partial t} + \frac{\partial r}{\partial t} = q_s, \quad (3)$$

where  $c$  is the average volume concentration,  $Q_s$  is the sediment volume flux,  $\lambda$  is the bed porosity,  $w$  is the active width of the bed (i.e., that portion of the bed width in which erosion or deposition takes place),  $z$  is the local bed elevation,  $r$  is the net sediment volume flux through the suspended-bed load interface, and  $q_s$  is the lateral inflow of sediment per unit channel length.

In Eq. 3 the third term represents the volume rate of sediment scour (or deposition) per unit length of channel bed. The fourth term is envisioned as the time rate of net local exchange between the suspended and bed load zones. An expression defining this term is needed for solving Eq. 3. For simplicity, the following parametric exchange equation is adapted (Whitham, 1974)

$$\frac{\partial r}{\partial t} = k_0 A [(1-c) - k_1 (R-r)c]. \quad (4)$$

Here  $k_0$  and  $k_1$  are constants,  $T$  is the concentration at transport capacity, corresponding to which,  $R$  is the net sediment exchange between the suspended and bed zones. Eq. 4 was so constructed in order to (i) incorporate in the solution some of the nonlinearity undoubtedly present in the exchange process, and (ii) preserve the hyperbolic character of the sediment continuity equation. Although Eqs. 3 and 4 can be solved by successive iterations to obtain  $c$  and  $r$ , a simpler solution results from the following observation. Very near equilibrium the right hand side of Eq. 4 vanishes for all practical purposes. That is

$$k_o A \{ (T-c)r - k_1 (R-r)c \} \approx 0 . \quad (5)$$

At the same time  $T$  deviates slightly from its equilibrium value. Thus, from Eq. 5 results

$$\frac{\partial r}{\partial t} = \frac{k_1 RT}{[T + (k_1 - 1)c]^2} \frac{\partial c}{\partial t} . \quad (6)$$

Also this expression is assumed to hold in slowly varying flow conditions. Approximating  $Q_s$  by AVC over a small time interval, and combining Eqs. 3 and 6 gives the sediment continuity equation used in this model

$$\frac{\partial c}{\partial t} + V_s \frac{\partial c}{\partial x} = \frac{q_{st}}{A(1+f_s)} , \quad (7a)$$

$$\text{where } V_s = \frac{V}{(1+f_s)} , \quad (7b)$$

$$f_s = \frac{k_1 RT}{A[T + (k_1 - 1)c]^2} , \quad (7c)$$

$$q_{st} = q_s - (1-\lambda)W \frac{\partial z}{\partial t} \quad (7d)$$

Eq. 7a is a quasilinear hyperbolic equation governing the propagation of the sediment concentration waves. Its right hand side represents the lateral sediment inflow contributed by runoff, tributary channels, and bed scouring. The limited experience gained so far with the model indicates that  $k_1$  is of order  $10^{-3}$ . Thus Eq. 7c has been approximated by,

$$f_s \approx \frac{CEL}{AT[1-0.999c/T]^2} , \quad (7e)$$

where CEL is a user supplied parameter. This parameter should be adjusted to match the time of arrival of the observed sediment load peak at the channel outlet. Eqs. 7b and 7e show that the celerity of the sediment wave,  $V_s$ , is controlled by the local hydraulic conditions and sediment properties since capacity depends on these parameters as well.

Eq. 7a can be solved by means of the method of characteristics. From this equation and the total differential of the sediment concentration, the following characteristic equations result

$$\frac{dx}{dt} = V_s , \quad (8a)$$

$$\frac{dc}{dt} = \frac{q_{st}}{A(1+f_s)} = -\frac{q_{st}}{Q} V_s . \quad (8b)$$

These equations show that Eq. 7a possesses only one system of forward characteristics. Accordingly, this equation cannot be used in situations where there are flow reversals. Integrating Eqs. 8a and 8b with the initial condition  $c_o = c(x_o, t_o)$  gives

$$c = c_o + \int_{x_o}^x \left( q_{st}/Q \right) d\xi , \quad (9a)$$

$$t = t_o + \int_{x_o}^x V^{-1}(1+f_s) d\xi . \quad (9b)$$

These integrals are used to track the evolution of the sediment waves across the characteristic plane. The concentrations existing on all the characteristics at the time of their arrival to the downstream boundary define the outflow sediment graph.

It is interesting to note that the preceding equations reflect the expected behavior. For instance, it is a recognized fact that the streamwise velocity of sediment particles always lags behind the velocity of the surrounding fluid (Francis, 1973). This velocity lag ranges from very small values for silt particles in suspension, to quite large differences in the case of coarse sands and gravels. Thus, the celerity of a sediment-load wave will be smaller, in general, than the celerity of the carrying flow wave. This trend is also predicted by Eqs. 7b and 7e, for they indicate that waves of coarse material will travel slower than waves of finer material given that the carrying capacity of a stream increases as the sediment size decreases.

This celerity lag is strictly a function of local flow and sediment properties, and it should not be confused with the differences sometimes

observed between the time of arrival of the flow and sediment load peaks. In fact, the sediment load may peak ahead, in phase, or behind the flow peak depending on antecedent conditions, intensity of the event, sediment source location, season of the year, etc. (Guy, 1970). To illustrate this point consider a channel reach having a deposit of very fine sediment on the upstream portion of the reach, and receiving an inflow  $Q_U$  as shown in Fig. 2a. The sediment will be entrained as soon as  $Q_U$  reaches a sufficient intensity, and will move along characteristics parallel to the flow characteristics (i.e.,  $V_s = V$ , Eq. 8a). As the characteristics reach the downstream boundary the water and sediment outflows begin to rise, generally at different rates. The concentration increase rate is controlled by the ratio of sediment entrainment to flow discharge (Eq. 8b). If the supply of loose sediment is finite, the sediment outflow will peak at some time  $t_2$ , while the water outflow will continue to increase and peak at a later time  $t_3$ . The lag between these two peaks will obviously depend on the magnitude of the sediment supply, inflow rates, and distance of sediment source to channel outlet ( $x = x_2$ , Fig. 2a). For simplicity, this example has ignored backwater effects to restrict the flow movement to forward characteristics. Next, consider the same channel reach but with the source located farther upstream and a constant base flow  $Q_U$  (Fig. 2b). The flows and sediment loads reaching the channel inlet ( $x = x_1$ ) are generated by characteristics emanating from the upstream reach,  $x_0 \leq x \leq x_1$ . Lateral runoff,  $q_w$ , is assumed to begin entering the channel at  $t = t_4$ . At this point the outlet hydrograph will begin to rise and eventually peak at  $t = t_5$ . On the other hand, the sediment characteristics, which enter the channel reach after  $t_4$ , will reach the outlet later than  $t_5$  and will finally peak at a later time  $t_6 > t_5$ . Thus, in this case the sediment peak lags significantly behind the flow peak as result of changes in the channel water inflow and sediment source location.

Consider now a channel with sediment moving mostly as bedload. In this case the term  $\partial r / \partial t$  in Eq. 3 can be neglected. Furthermore, Mahmood (1975) has shown that ignoring the time derivative of the spatial concentration has little influence on the simulation of bedload propagation. If in addition the period of the flow velocity field is very large, the surface gravity waves can be filtered out and only the

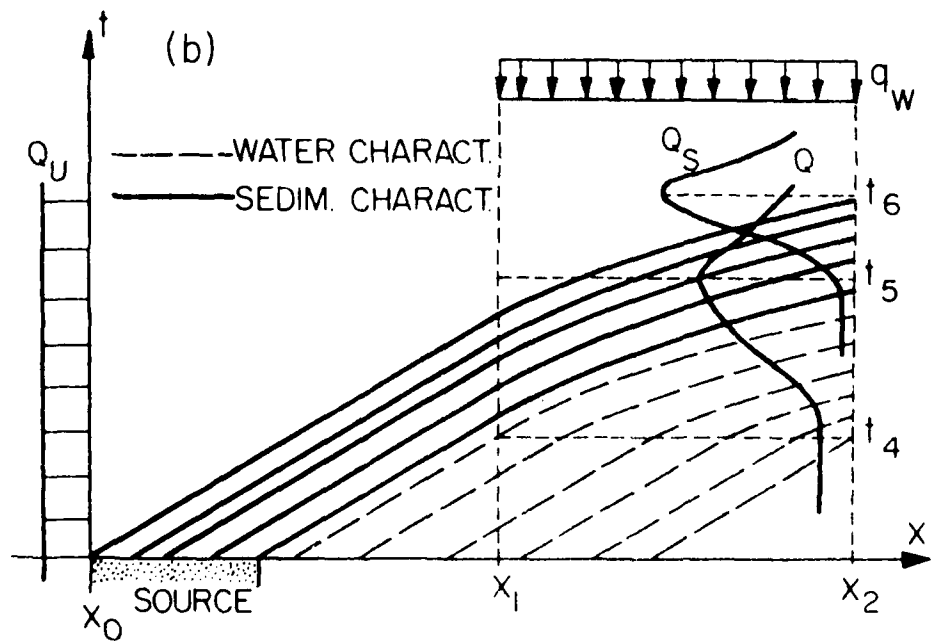
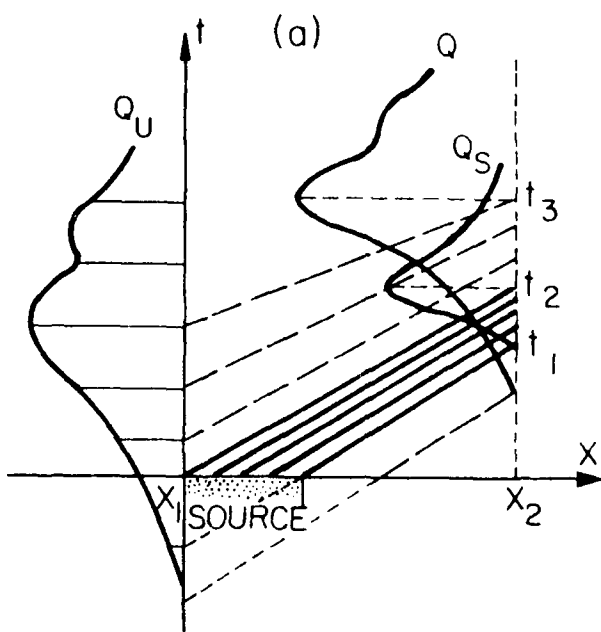


Fig. 2. Routing of water and sediment characteristic waves

bedload propagation waves need be retained (Gradowczyk, 1968). In such an instance, Eqs. 1, 2, and 3 reduce to the equations governing the "known discharge" approximation frequently employed in modeling propagation of bed transients (Gradowczyk, 1968; de Vries, 1971; Cunge and Perdreau, 1973; Thomas and Prashun, 1977; Ponce et al., 1979).

The foregoing observations demonstrate that the equations presented in this Section incorporate the ingredients needed to simulate the actual physical process. These equations are complemented with a number of ancillary algorithms discussed in the following sections.

In natural channels there is usually a wide gradation of sediment sizes. Although the finer particles comprise the bulk of the load, the channel evolution is controlled by the coarser particles (i.e., armor-ing). Moreover, different sizes are transported at different rates as pointed out earlier. It is thus important to predict the movement of the individual particle sizes encountered in the channel. The present model divides the size range in a suitable number of size fractions, and then uses Eqs. 7b, 7d, 7e, and 9 to track the movement of each fraction.

## 2.2 ANCILLARY ALGORITHMS

### 2.2.1 Sediment Transport Formulas

These formulas are used to determine the potential carrying capacity of a specific flow. Different capacities can be expected for different particle sizes, and not all existing formulas perform equally well for all sizes. In the present model several formulas are used that are framed for easy use in digital applications, and require only information on the hydraulic parameters of the carrying flow. They are the total load formula of Yang (1973) used to estimate the transport of very fine to coarse sands (0.1-2 mm), a duBoys-type bedload formula (Graf, 1971) used with fine gravel particles (2-4 mm), and the Meyer-Peter and Muller bedload formula (Meyer-Peter and Muller, 1948) used with particles in the medium to very coarse gravel range (4-65 mm). These formulas are presented in Addendum 2 in the forms used in this model. The Yang formula was found to give very reliable estimates for flows carrying sands in the indicated size range, including flows transporting sediment mostly as bed load (Alonso et al., 1980). The duBoys-type formula and the Meyer-Peter and Muller formula were selected because they were developed from data in the specified size ranges.

Nevertheless, the user may replace these formulas by others he may deem more appropriate for a particular simulation. In particular, simple relationships between the sediment transport rate and the flow condition developed from in situ field surveys should be given preference.

#### 2.2.2 Residual Capacity. Composition of Material in Transport

Whenever the bed material consists of a mixture of different sediment sizes, the particle size composition of the sediment discharge usually differs from that of the bed. Therefore, the transport must be characterized by a load rate and a size distribution analysis. Although a flow may have the potential to transport sediment, its residual capacity or ability to carry any additional load depends on the sediment material already present in the flow. Consider, for instance, a flow carrying a load  $c_1$  of uniform size  $d_1$  and let  $T_1$  be the corresponding potential capacity of the flow. Then

$$T_{r1} = T_1 - c_1 = T_1 - T_1 (c_1/T_1)$$

is the residual capacity of the flow for that size material. The last term in this expression represents that portion of  $T_1$  already consumed by the material in transport. Similarly, if the later were of a different size  $d_2$ , the residual capacity for the size  $d_1$  material, in the presence of the load  $c_2$ , would be

$$T_{r1} = T_1 - T_1 (c_2/T_2) ,$$

where  $c_2/T_2$  may be envisioned as that part of  $T_1$  depleted by the load  $c_2$ . If both sizes were simultaneously present in the flow, then

$$T_{r1} = T_1 - T_1 (c_1/T_1) - T_1 (c_2/T_2) .$$

This expression can be generalized to any size fraction,  $d_i$ , and for an arbitrary number,  $n$ , of load fractions  $c_1, c_2, \dots, c_n$ , as follows

$$\begin{aligned} T_{ri} &= T_i - T_i (c_1/T_1) - T_i (c_2/T_2) - \dots \\ &\quad - T_i (c_i/T_i) - \dots - T_i (c_n/T_n), \end{aligned} \quad (10)$$

or,

$$T_{ri} = T_i [1 - \sum_{j=1}^n (c_j/T_j)] = \Delta T_i, \quad i = 1, 2, \dots, n . \quad (11)$$

The quantity within brackets,  $1 - \sum_{j=1}^n (c_j/T_j)$ , represents the portion of the potential capacity  $T_i$  taken up by all the size fractions in transport. Therefore, the quantity within brackets,  $\Delta$ , is the remaining capacity for transporting additional material of size  $d_i$ . For a given sediment load,  $\Delta$  is the same for all fractions.  $T_i$  depends uniquely on the local flow and the properties of the  $d_i$  fraction, while  $T_{ri}$  depends on all these parameters and on the size composition of the sediment load.

When  $\Delta > 0$ , any size fraction available for entrainment at the bed surface, and for which  $T_i \neq 0$ , will be removed by the flow and added to the same sediment size class already in transport. Thus,  $\Delta > 0$  identifies an eroding bed condition. Similarly, when  $\Delta < 0$  the stream carries a load in excess of its potential capacity and will deposit the excess sediment material on the bed. Therefore,  $\Delta < 0$  characterizes an aggrading bed condition. When  $\Delta = 0$  there is no load change and the transport process remains in a pseudo-equilibrium condition. By continuously tracking the value of  $\Delta$ , the dependence of the individual residual capacities on the composition of the sediment load and its exchange with the bed is readily simulated.

The size composition of the total load is continuously up-dated by adjusting the concentration of individual fractions according to the composition of the material removed from or added to the bed. This procedure is explained later in the report.

#### 2.2.3 Bed Composition

In cohesionless beds the material available for entrainment is essentially that exposed at the bed surface. As dunes and ripples move slowly downstream they continuously mix all the sediment they contain. The space occupied by those bed features may thus be regarded as a mixing zone below which the bed material remains undisturbed (Fig. 3a). Where the sediment contains a mixture of different sizes, the slowly moving coarse material tends to collect at the base of the mixing zone thus forming a lens of large grains. Under some flow conditions the coarse material in the bed may become immobile. In this case, the flow washes the finer particles out of the mixing zone leaving an armor coat that protects the underlying material. During the scouring of the finer materials the exchange between bed and flow takes place in a thin layer

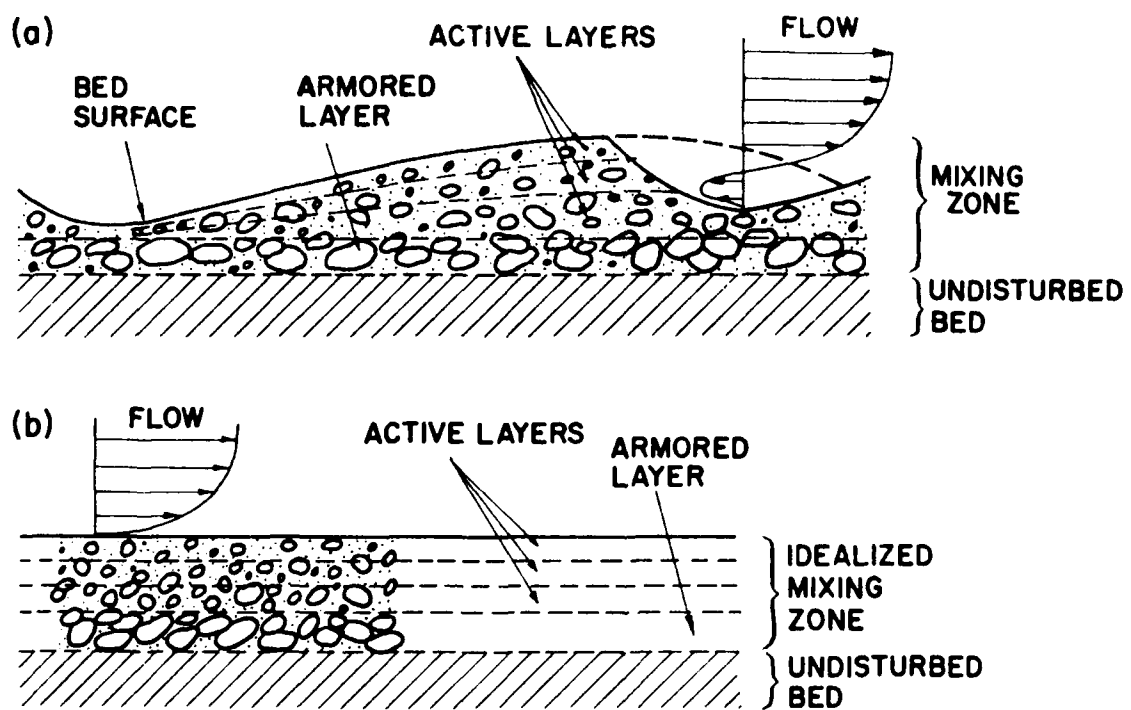


Fig. 3. Schematic representation of bed processes

at the bed surface, identified here as the active layer. Several of these layers will be scoured away while the mixing zone is degrading. When the bed is armored, the last active layer becomes the armor coat. Conversely, during the process of bed aggradation several active layers will be deposited on the bed forming a new mixing zone.

To model the above processes the mixing zone is pictured as a band of constant thickness divided into several layers (Fig. 3b). The layer in contact with the flow is always referred to as the active layer. The thickness, porosity, and size distribution of this layer can vary throughout the simulation, but the layer is assumed to be homogeneous within itself at any given time.

When all the material within the active layer moves, a reasonable upper bound of its thickness is obtained, from volumetric considerations, as

$$ALT = \frac{100}{P_n} \frac{d_n}{1-\lambda_n} \quad (12)$$

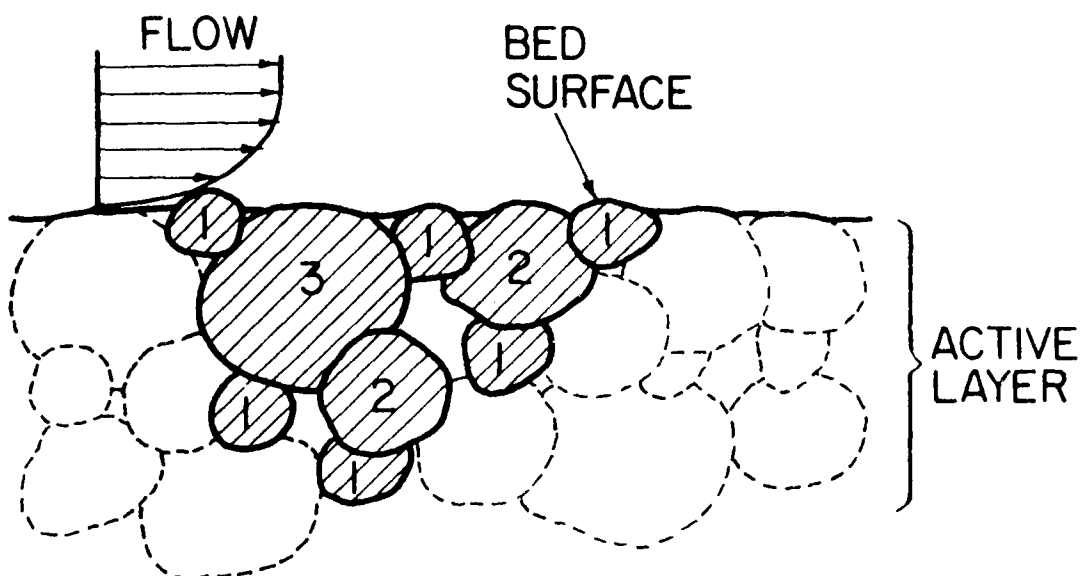
Here  $d_n$ ,  $P_n$ , and  $\lambda_n$  are the size, percentage, and porosity of the coarsest fraction in the sediment mixture. For instance, in a uniform bed material with  $\lambda_n = 0.50$ , Eq. 12 gives  $ALT = 2d_n$  which is in agreement with the bed load thickness proposed by Einstein (1950). However, when the active layer becomes an armor coat, its actual thickness may be considerably less than that predicted by Eq. 12 because the bed may be armored by particles smaller than  $d_n$ . In that case, it is proposed to compute the layer thickness from

$$ALT = \frac{100}{\sum_{i=\ell}^n P_i} \times \frac{d_\ell}{1-\lambda_\ell} \quad (13)$$

where  $d_\ell$  is the smallest grain fraction the flow cannot transport (i.e.,  $T_i=0$ ,  $i = \ell, \ell+1, \dots, n$ ). Eq. 13 is also a better measure of the active layer thickness when some of the fractions in the bed layer cannot be eroded by the flow. At low discharges only the smaller fractions will be set in motion and Eq. 13 will thus predict a thin active layer. This

is intuitively correct since little bed material will be scoured by a low flow during a simulation time step. As the discharge increases, the coarser fractions, usually present in small percentages, will be entrained and Eq. 13 will predict a thicker layer. This behavior is in agreement with the fact that a greater depth of bed can be sorted through by a higher flow in the same amount of time. Eq. 13 is thus adopted as the general expression for the active layer thickness. This equation incorporates Eq. 12, in the limit, by letting  $\ell = n$  when all fractions are in motion. The sediment contained in the active layer is the only material available for erosion during a simulation time step. When the bed is armored no erosion can occur until the flow develops the necessary  $T_r$  for the smallest size fraction present in the armor coat. When this happens the armor coat becomes again an eroding active layer. If deposition of a certain amount of sediment occurs during simulation, this material is added to the bed and a new active layer thickness is computed based on the new mixture composition.

In order to account for the time evolution of the active layer thickness, it is necessary to continuously track the size composition of this layer. This is done by introducing the following accounting algorithm. Consider a well mixed active layer with three size fractions  $d_1 < d_2 < d_3$  being eroded by a flow with sufficient transport capacity to scour all three fractions (Fig. 4). The bed scouring is imagined to begin with the entrainment of the  $d_1$ -particles exposed at the bed surface. Next, the  $d_2$ -particles at the bed surface are removed, followed by the  $d_1$ -grains hidden underneath the  $d_2$ -grains. Finally, the  $d_3$ -particles are washed off the bed surface followed by the  $d_1$  and  $d_2$ -particles underneath them, and by the  $d_1$ -grains uncovered by the removal of the  $d_2$ -grains. Thus, one  $d_1$ -particle is removed for every  $d_2$ -particle entrained by the flow, and one  $d_2$  and two  $d_1$ -grains are associated with the removal of every  $d_3$ -grain. This ordering can be readily extended to a  $y$  number,  $n$ , of size fractions, and it is summarized in the following "entrainment frequency" matrix.



NOTE NUMBERS IDENTIFY PARTICLES BELONGING  
TO DIFFERENT SIZE FRACTIONS.

Fig. 4. Schematic representation of active layer composition

$$\tilde{F} = [F_{ij}] = \begin{bmatrix} 1 & 0 & 0 & 0 & \dots & 0 & \dots & 0 \\ 1 & 1 & 0 & 0 & & & & 0 \\ 2 & 1 & 1 & 0 & & & & 0 \\ 4 & 2 & 1 & 1 & & & & 0 \\ 8 & 4 & 2 & 1 & & & & 0 \\ 16 & 8 & 4 & 2 & & & & 0 \\ 32 & 16 & 8 & 4 & & & & 0 \\ \vdots & \vdots & \vdots & \vdots & & & & \vdots \\ \vdots & \vdots & \vdots & \vdots & & & & \vdots \\ \vdots & \vdots & \vdots & \vdots & & & & \vdots \\ 2^{i-2} & 2^{i-3} & 2^{i-4} & 2^{i-5} & \dots & 2^{i-j-1} & \dots & 1 \end{bmatrix} \quad (14)$$

where  $i, j = 1, 2, 3, \dots, n$ . In this matrix the diagonal elements indicate that every size fraction at the bed surface is scoured once. The off-diagonal elements in each row indicate the number of times each fraction  $d_j$ ,  $1 \leq j \leq i$ , becomes available for entrainment once  $d_i$  is removed from the bed. Alternatively, the elements of any column,  $j$ , express the number of times the  $d_j$  fraction is depleted due to the entrainment of a fraction  $d_i$ . Obviously, the set of entrainment events in Eq. 14 is one of many possible distributions since in actuality any number of  $d_j$ -particles can be associated with the removal of a  $d_i$ -grain. In a more general stochastic representation the  $\tilde{F}$  matrix would be replaced by the conditional probability matrix of the entrainment process. Nevertheless, the proposed algorithm is adopted for its deterministic simplicity. It should be noted that the  $\tilde{F}$  matrix is time invariant and depends only on the number of fractions used in the simulation.

The amounts of eroded materials corresponding to the frequencies  $F_{ij}$  depend on the volumes of the fractions contained in the active layer. To convert those frequencies to volumes let  $V_j$  be the total volume of the  $d_j$ -size present in the layer per unit channel length, and  $v_{ij}$  the portion of  $V_j$  that becomes available for entrainment when the  $d_i$ -fraction, occupying the volume  $V_i$ , is eroded. Thus,

$$v_{ij} = F_{ij} V_i ,$$

$$V_j = \sum_{r=j}^n F_{rj} V_r ,$$

from which,

$$v_{ij} = \frac{F_{ij} V_i}{\sum_{r=j}^n F_{rj} V_r} \times V_j . \quad (15)$$

From this expression one obtains

$$\sum_{i=j}^n v_{ij} = V_j . \quad (16)$$

Eq. 15 can be rewritten as

$$v_{ij} = \frac{F_{ij} P_i}{\sum_{r=j}^n F_{rj} P_r} \times V_j , \quad i, j = 1, 2, \dots, n , \quad (17)$$

where,

$$P_i = \frac{100 V_i}{\sum_{k=1}^n V_k} , \quad i = 1, 2, \dots, n , \quad (18)$$

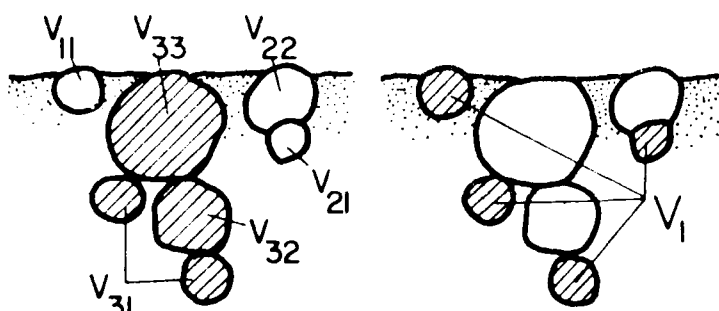
are the percentages of active-layer material in each size class interval.

Eq. 17 defines the elements of a square matrix identified in here as the "volume entrainment matrix,"  $v$ . The order of this matrix is equal to the total number of size classes in the active layer. Its diagonal elements represent the volumes of the individual fractions on the bed surface. The off-diagonal row elements contain the individual fractional volumes exposed by the erosion of larger sizes. Adding up these elements gives the volume of potential erosion associated with the removal of the largest size in the row. On the other hand, summing all the elements in each column yields the total volume of each size class present in the active layer and available for scour (Eq. 16). These concepts are schematically illustrated in Fig. 5a, which depicts the  $v$ -matrix associated with a small cluster of bed particles grouped in three different size classes. The shaded area in Fig. 5b represents all the material that could be entrained along with the third fraction. The shaded portion of Fig. 5c represents instead the total volume of the first fraction contained in the cluster. During bed degradation, or aggradation, the elements of the  $v$ -matrix are continuously adjusted as

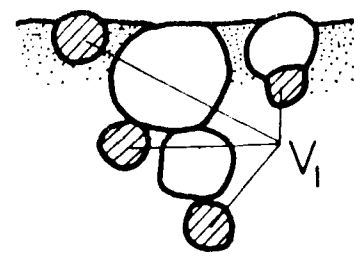
$v_{11}$	0	0
$v_{21}$	$v_{22}$	0
$v_{31}$	$v_{32}$	$v_{33}$

$V_1 \quad V_2 \quad V_3 = \sum_i v_{ij}$

(a)



(b)



(c)

Fig. 5. Graphical representation of  $\underline{v}$ -matrix components

explained in the next two sections. At the end of each simulation time step the total volumes of the individual fractions left in the active layer are introduced into Eq. 18 to calculate the size distribution of the layer.

#### 2.2.4 Bed Erosion. Armoring

Whenever  $\Delta > 0$  the bed is in a degrading mode. This is conceptually modeled by depleting the elements of the  $\underline{y}$ -matrix, one row at a time, beginning from the smallest fraction. The diagonal elements are depleted first, for they are exposed to the flow when simulation starts. Next, the off-diagonal elements are scoured one by one beginning from the smallest size. When the flow residual capacity is not sufficient to remove all the volumes in a particular row, equal amounts (for simplicity) are removed from all the elements in the row until the residual capacity is satisfied. The eroded volumes are added to the individual fractions already in transport, and the value of  $\Delta$  is recalculated. This process continues until either  $\Delta$  is no longer positive definite, or the entire active layer is worked through. For example, the volumes ( $v_{11}$ ), ( $\frac{1}{2}v_{22}$ ,  $\frac{1}{2}v_{21}$ ;  $\frac{1}{2}v_{22}$ ,  $\frac{1}{2}v_{21}$ ; etc.), ( $v_{33}/3$ ,  $v_{31}/3$ ,  $v_{32}/3$ ;  $v_{33}/3$ ,  $v_{31}/3$ ,  $v_{32}/3$ ; etc.) would be eroded, in this order, out of the  $\underline{y}$ -matrix shown in Fig. 5. However, the extent to which these volumes are actually entrained depends on the degree of detachability of the sediment particles. These concepts are used to construct the following algorithm expressing the total volume of sediment eroded out of each size class in the active layer during a simulation time step:

$$E_i^* = \left\{ \sum_{j=1}^i e_{ij}, e_{ij} = ERO \cdot v_{ij}, \text{ if } AT_{ri} \geq \sum_{j=1}^i v_{ij}, \right. \quad (19a)$$

$$\left. \sum_{j=i+1}^{r-i} e_{ij}, e_{ij} = \begin{cases} \frac{1}{i} ERO \cdot v_{ij}, & \text{if } j \leq r, AT_{ri} = \sum_{j=1}^r v_{ij}, \\ AT_{rj} \geq \frac{1}{i} v_{ij}, & \end{cases} \right. \quad (19b)$$

$$\left. \begin{cases} ERO \cdot AT_{rj}, & \text{if } j = r, AT_{ri} = \sum_{j=1}^{r-i} v_{ij}, \\ AT_{rj} < \frac{1}{i} v_{ij}, & \end{cases} \right. \quad (19c)$$

$i=1, 2, \dots, n$ . In these equations ERO is a user supplied erodibility parameter. This parameter governs the actual amount of bed material available for erosion during a simulation time step. ERO is calibrated by fitting the sediment yield volume to observed data. Everytime a new  $e_{ij}$  is computed the concentration of the corresponding load fraction,  $c_j$ , is upgraded by letting

$$c_j^* = c_j + \frac{e_{ij}}{A}. \quad (20)$$

This concentration is then entered in Eq. 10 to update  $\Delta$ . When  $\Delta$  becomes nonpositive for any particular size fraction the transport is termed "capacity limited." On the other hand, if  $\Delta$  remains positive after depleting a fraction the situation is termed "supplied limited." In particular, if  $\Delta > 0$  after considering all fractions present in the active layer, the bed is said to be armored and the active layer becomes an armor coat. Fig. 6 summarizes the foregoing simulation sequence.

After the active layer has been worked through by the flowing water, its volumetric composition is given by  $V_i - E_i^*$ ,  $i=\ell, \ell+1, \dots, m$ , where  $\ell$  and  $m$  are the smallest and largest fractions left in the layer. The actual thickness of this material is then

$$ALT^* = \frac{1}{W} \sum_{i=\ell}^m \frac{V_i - E_i^*}{1 - \lambda_i}. \quad (21)$$

Whenever  $ALT^*$  is equal, or larger, than the thickness obtained from Eq. 12, the later is taken as the new thickness of the active layer. In some instances, however,  $ALT^*$  turns out smaller than  $ALT$ . In these cases, a thickness,  $\delta$ , of undisturbed material is added to the active layer (Fig. 7a). Because the model does not track the composition of the undisturbed layer, this is always formed by original bed material. This material contains, in general, a smaller percentage of the largest size class than the  $ALT^*$  layer (Fig. 7b) and, therefore,  $\delta$  must be reduced to account for the difference. For simplicity, a simple linear correction is assumed given by the ratio between the percentages,  $P_m^a$  and  $P_m^u$ , in the eroded and undisturbed layers (Fig. 7b). Thus, the corrected thickness of the new active layer becomes

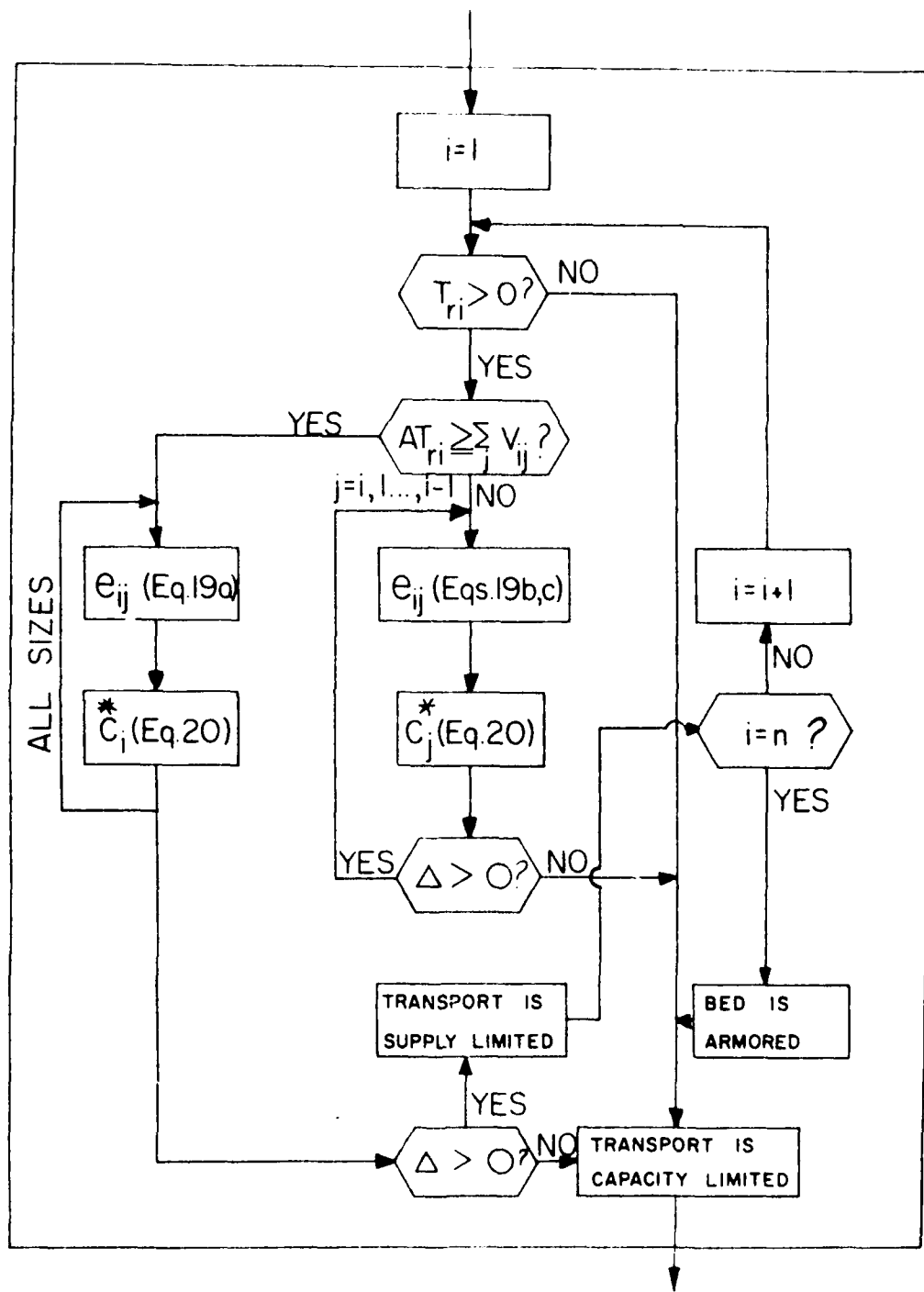


Fig. 6. Erosion loop

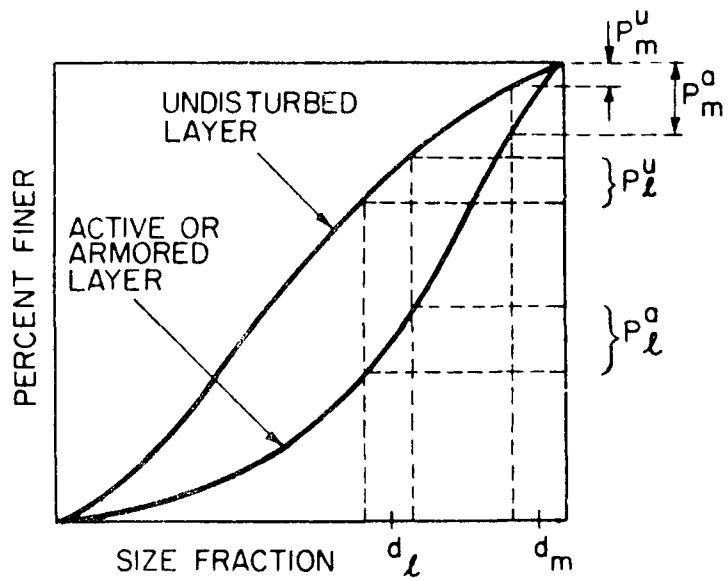
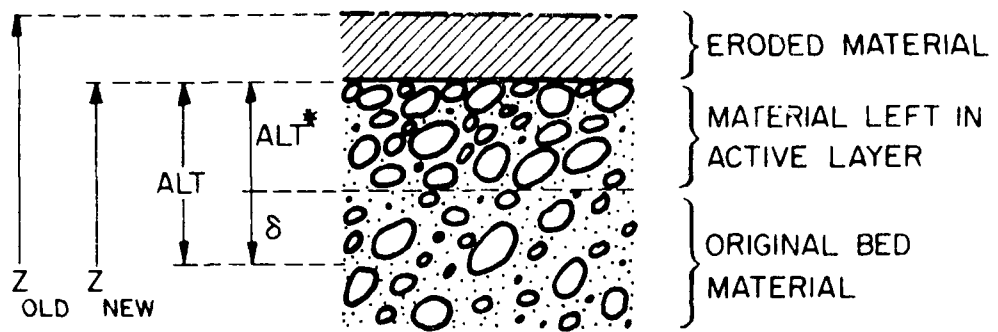


Fig. 7. Adjustment of active-layer thickness

$$ALT_c = ALT^* + \delta \frac{P_m^a}{P_m^u}. \quad (22)$$

The same criteria is used when updating an armor coat thickness, except that in this case the ratio  $P_m^a/P_m^u$  is replaced by  $P_\ell^a/P_\ell^u$ .

Finally, the local bed elevation of the channel bed is updated by subtracting from it the thickness of the eroded material, giving (Fig. 7a)

$$z_{\text{new}} = z_{\text{old}} - \frac{1}{W} \sum_{i=1}^n \frac{E_i}{(1-\lambda_i)}. \quad (23)$$

#### 2.2.5 Sediment Deposition

When the model senses deposition ( $\Delta < 0$ ), the flow drops sediment on the bed during the time step,  $\Delta t$ , and the settled material is added to the active layer. Within the present deterministic framework, deposition begins with the largest sediment fraction and continues through the smaller fractions until either the stream is no longer overloaded ( $\Delta = 0$ ), or all the fractions in transport have been depleted. The volume deposited out of any fraction,  $D_i$ , cannot exceed its (defect) residual capacity, that is,

$$\text{Maximum } D_i = T_{ri} = T_i \Delta. \quad (24)$$

However, whether this amount will reach the bed during the time step  $\Delta t$  depends on this being not less than the average time for the sediment particles to settle to the channel bed. Data by Jobson and Sayre (1970) and by Lean (1971) indicate that this settling time may be computed using the particle fall velocities in the quiescent fluid. Therefore, the actual deposition of a size fraction during the interval  $\Delta t$  is calculated from

$$D_i = \begin{cases} T_i \Delta, & \text{if } \beta \geq 1, \\ \beta T_i \Delta, & \text{if } \beta < 1, \end{cases} \quad (25)$$

where  $\beta = 2w_i \Delta t / h$ ,  $h$  is an average flow depth for the reach (see Fig. 11), and  $w_i$  is the fall velocity of the individual fraction. The settling length  $h/2$  has been used in Eq. 25 because not all sediment

particles fall simultaneously from the water surface. The deposited volume  $D_i$  is subtracted from the material in transport to yield the size-class concentration

$$c_i^* = c_i - \frac{D_i}{A}. \quad (26)$$

From the preceding equations the deposition loop shown in Fig. 8 is constructed.

The settled sediment is added to the active-layer fractions, and both materials are assumed to mix thoroughly yielding the volumetric composition

$$v_i^* = \begin{cases} v_i, & \text{when } D_i = 0, \\ v_i + D_i, & \text{when } D_i \neq 0, \end{cases} \quad (27)$$

$i = 1, 2, \dots, n$ . These volumes are introduced in Eq. 17 to update the bed composition, and this is then used in Eq. 12 to compute the new active layer thickness. Finally, the local bed elevation is updated by adding to it the thickness of the settled material yielding

$$z_{\text{new}} = z_{\text{old}} + \frac{1}{W} \sum_{i=1}^n \frac{D_i}{(1-\lambda_i)}. \quad (28)$$

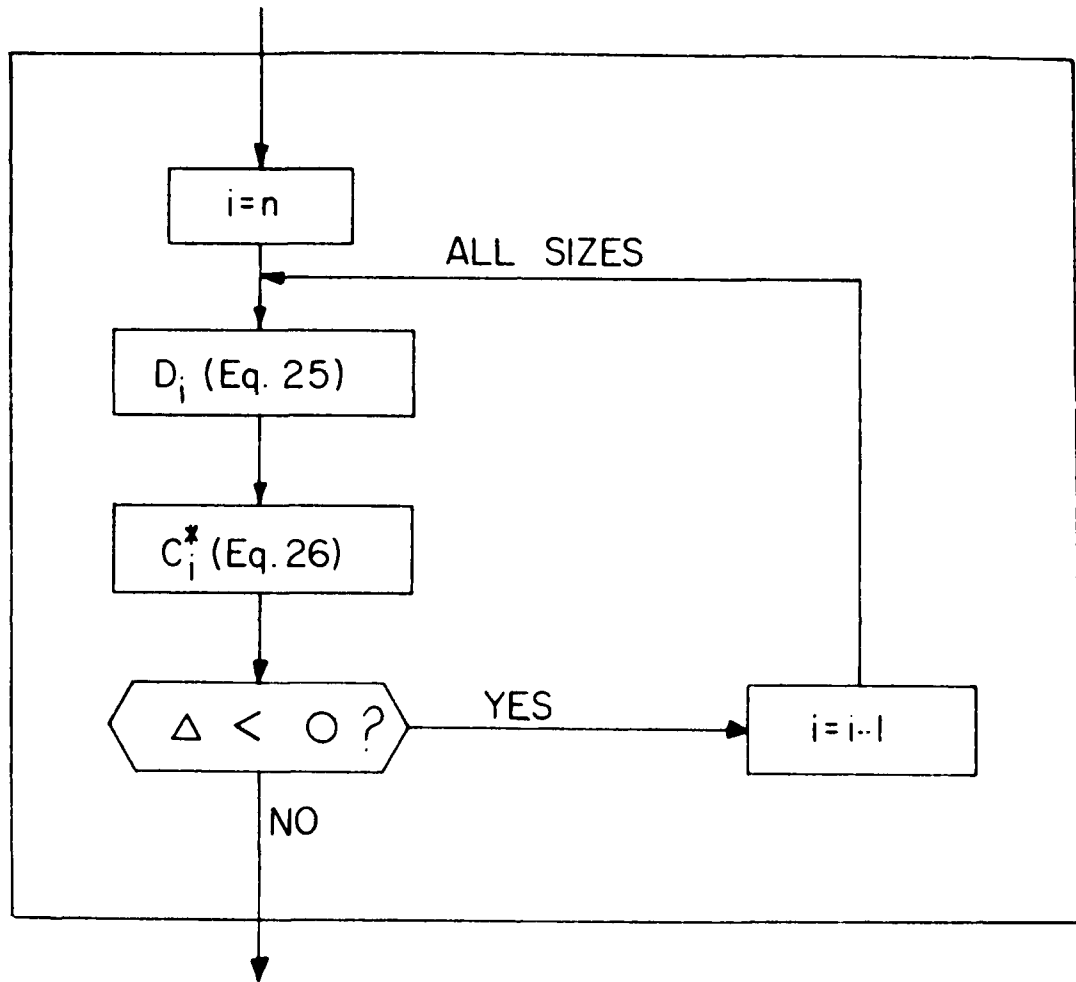


Fig. 8. Deposition loop

## NUMERICAL SCHEME

To run the model in a channel reach of length  $L$ , the open domain  $[0 \leq x \leq L] \times [t \geq 0]$  is covered with a rectangular grid with lines parallel to the  $x$ - and  $t$ -axes. There is a single family of characteristics associated with Eq. 7a. This leads to the solution of an initial, one-point boundary value problem. Initial conditions are cross-section geometry, bed elevation, average flow velocities, flow depth, active width, and bed size composition. Upstream boundary conditions are time histories of water and sediment inflow, and size composition of sediment load. Let  $\Delta x$  and  $\Delta t$  be the length and time increments, respectively, separating the grid lines (Fig. 9). The coordinates of the grid nodes are  $x_m = m\Delta x$  and  $t_n = n\Delta t$ ,  $m, n = 0, 1, 2, \dots$ . The value of any variable, say  $A$ , at the node  $(x_m, t_n)$  is designated  $A_m^n$ . Given the above data specified along the line  $t = t_n$ , the model is used to compute the sediment discharge, load composition, bed elevation, and active layer composition at all nodes on the next line  $t = t_{n+1}$ . For use in the numerical scheme, the sediment transport equations and ancillary algorithms are implemented as shown in the diagram of Fig. 11.

The volumes of the sediment fractions available for erosion during  $\Delta t$  are obtained from the active layer thicknesses on the line  $t = t_n$  as

$$V_{i,m}^n = \frac{W_m^n}{100} \frac{ALT_m^n}{1-\lambda_i} P_{i,m}^n, \quad i = 1, 2, \dots, n. \quad (29)$$

These volumes are used in Eq. 17 to compute the volume entrainment matrix  $V_m^n$ .

The flow routing scheme supplied by the user is used to obtain the hydraulic-parameter values at the nodes J and K (Fig. 9), and their averages are used to compute an average transport capacity,  $\bar{T}$ . The concentration of each load fraction at the end of the characteristic path is obtained from the following discrete form of Eq. 9a

$$c_{i,B} = c_{i,m}^n + \frac{q_{st} \Delta x}{\bar{Q}}, \quad (30)$$

where  $\bar{Q}$  is the average of  $Q_J$  and  $Q_K$ , and  $q_{st}$  is the piecewise uniform lateral sediment inflow over  $\Delta x$ . The amount of sediment entrainment, or

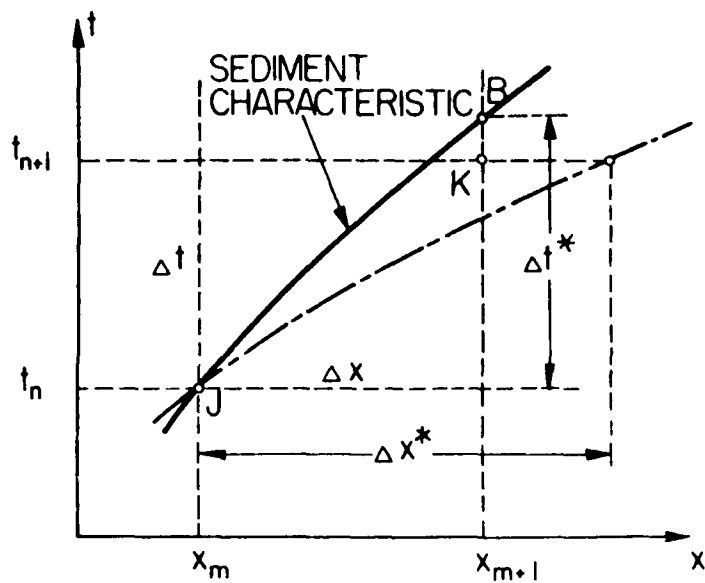


Fig. 9. Grid used in sediment characteristic solution

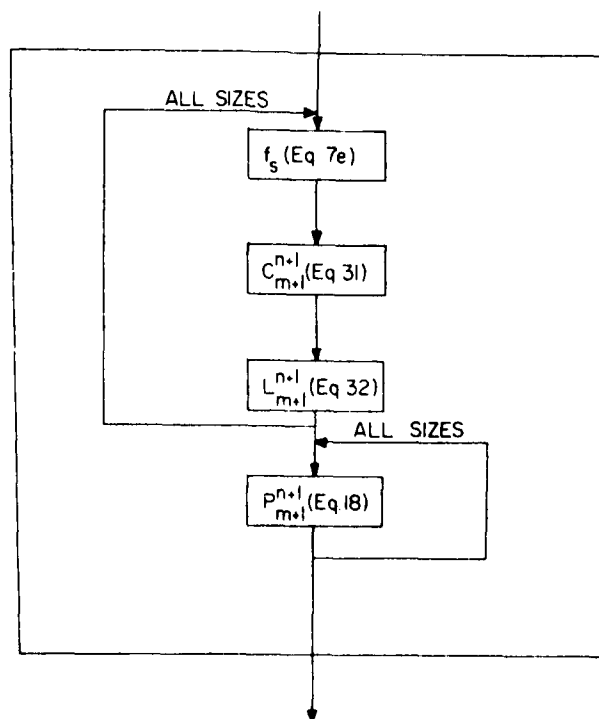


Fig. 10. Load updating loop

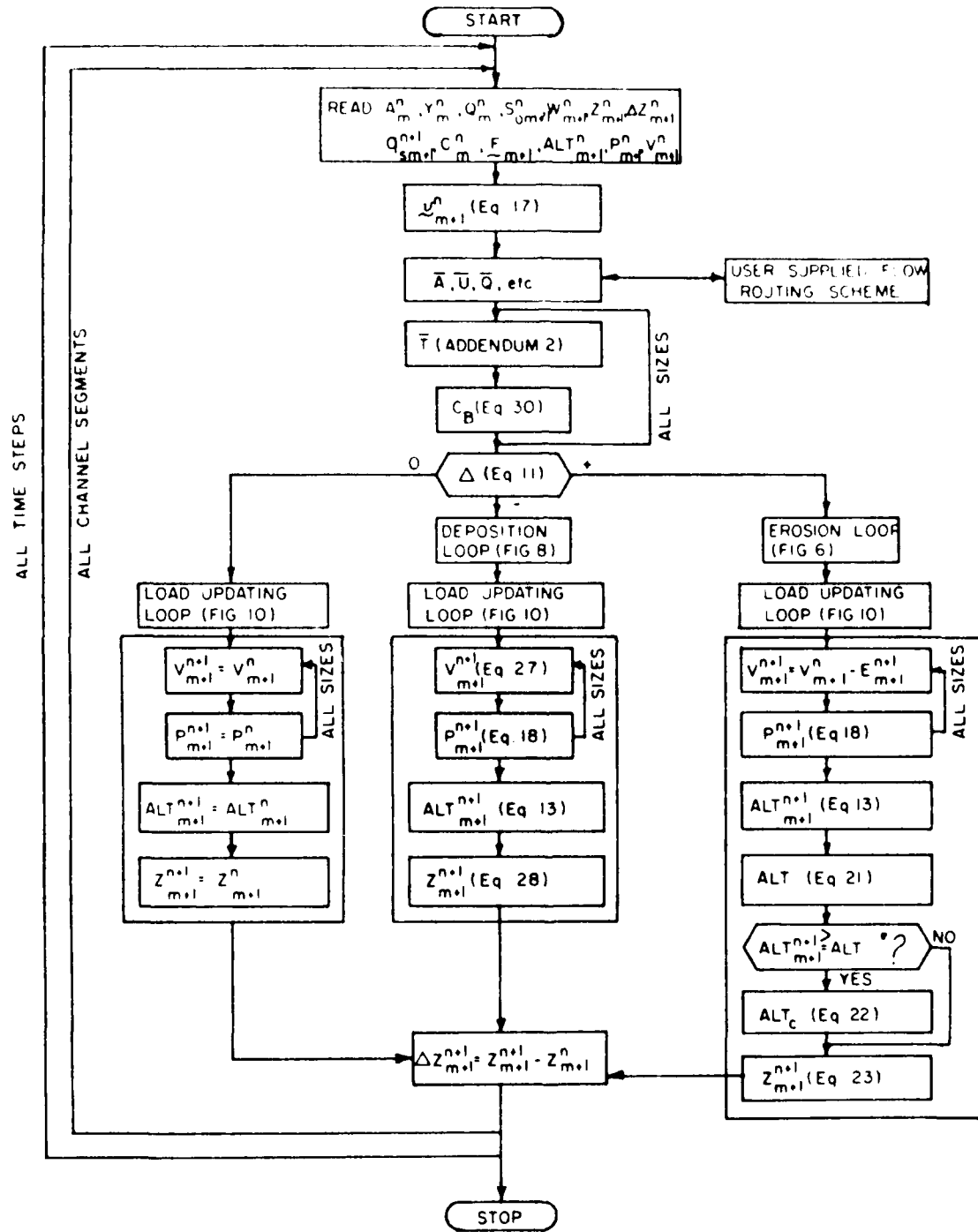


Fig. 11. Organization of numerical scheme

deposition, and the updated load concentration,  $c_{i,B}^*$ , are calculated using either the erosion loop (Fig. 6) or the deposition loop (Fig. 8) depending on the sign of  $\Delta$ . If the characteristic of a particular fraction does not pass through the node  $K$  (Fig. 9), the concentration at this node is obtained by linear interpolation from

$$c_{i,m+1}^{n+1} = \begin{cases} c_{i,B}^* \frac{\Delta t}{\Delta t^*} = c_{i,B}^* \frac{\Delta t}{\Delta x(1+f_{s,i})}, & \text{if } \Delta t^* > \Delta t, \\ c_{i,B}^* \frac{\Delta x}{\Delta x^*} = c_{i,B}^* \frac{\Delta x(1+f_{s,i})}{\Delta t}, & \text{if } \Delta t^* < \Delta t. \end{cases} \quad (31a)$$

In these equations  $\Delta x^*$  and  $\Delta t^*$  are given by discrete forms of Eq. 9b. A similar correction is applied to  $E_i^*$  (Eq. 19) to determine the actual amount of material eroded in the interval  $\Delta t$ . The new concentrations are used to calculate the new volume load fractions

$$L_{i,m+1}^{n+1} = \bar{A} c_{i,m+1}^{n+1}, \quad (32)$$

and these are introduced into Eq. 18 to update the load size composition. The foregoing load updating sequence is summarized in Fig. 10. Last, the new bed size composition and elevation are computed. When a pseudo-equilibrium condition is encountered ( $\Delta = 0$ ) no bed updating is necessary. In continuous simulation the above calculations are performed consecutively for each channel segment to update all variables over the length of the channel. The process is then repeated for each time interval in the simulation period.

## MODEL TESTING

Tests were conducted to verify the ability of the model to simulate various instream processes. Published laboratory and field studies were scanned for data suitable for testing the algorithms describing processes of bed scour, armoring, and unsteady transport. Three useful sets of data were found. The first set was collected by Ashida and Michiue (1971). They performed a series of laboratory experiments to study the effect of sediment gradation on channel armoring. The second data set was collected by Lane and Carlson (1953) in the San Luis Valley canals in south-central Colorado. They made measurements on the bed and bank materials that formed the canals. The beds of these canals have become armored over the years. The data offer an excellent opportunity for testing the model on a natural system. Finally, the model was tested using data collected by the U. S. Geological Survey on a reach of the East Fork River, Wyoming (Mahoney et al., 1976). These data offer the opportunity of checking the model algorithms on an alluvial stream under conditions of unsteady flow. These tests are discussed below.

As is usual in channels with material consisting of a wide range of grain sizes, the bed slopes of the channels used in the above three studies were fairly steep. In these cases the kinematic-wave approximation to the equations governing unsteady flow of water is applicable. In this approximation the momentum equation, Eq. 1, becomes

$$Q = KIN \cdot A^{3/2} P^{-1/2}, \quad (33)$$

where

$$KIN = C_f \cdot S_o^{1/2} = \frac{1.49}{n} R^{1/6} S_o^{1/2}, \quad (34)$$

is a kinematic-wave parameter. In these relationships  $P$  and  $R$  are the wetted perimeter and hydraulic radius of the channel cross section, respectively,  $C_f$  is the Chézy coefficient, and  $n$  is the Manning roughness factor. Eqs. 33 and 34 are also valid when the flow is uniform and steady. For the purpose of simulating the East Fork River data Eqs. 2, 33, and 34 were solved using the kinematic-wave routing scheme developed by Borah et al. (1980).

The simulations required calibration of the model parameters to obtain best-fit of model predictions to observations. One flow routing

parameter, KIN, and two sediment transport parameters, CEL and ERO, were available for adjustment. CEL controls the travel time of sediment load, and ERO governs the total quantity of bed material available for entrainment at the bed active layer.

#### 4.1 FLUME ARMORING STUDY

Several laboratory experiments were carried out by Ashida and Michiue (1971) to study the effects of bed armoring on channel degradation. Various sediment mixtures were used with different mean diameters and geometric standard deviations. These mixtures were placed in a recirculating flume with a bed 2.62 ft. wide and 65.5 ft. long. In each experiment a steady uniform flow was passed over the bed. The hydraulic conditions were chosen to purposely induce armoring. No additional sediment was introduced into the stream, and the rate of sediment collection in a trap at the end of the flume was used as a measure of the total sediment discharge.

Data from Ashida and Michiue's run No. 2 were chosen to check the performance of the model in simulating the transport of cohesionless sediment mixtures and the formation of armoring. The hydraulic conditions used in the run are given in Table 1. In running the model, the flume was represented by four reaches of equal length with a point inflow of water at the upstream end of the channel. The initial particle size distribution of the bed material employed in the run is shown in Fig. 12. In simulating sediment transport, the graded bed material was represented by ten discrete particle size fractions. They are listed in Table 2. Fig. 12 shows the size distributions of the eroded material leaving the flume and of the armoring layer as reported by Ashida and Michiue, and the best-fit curves predicted by the model. The agreement between the simulated and the measured armored layer size distributions is good. However, some discrepancy exists between the curves for the eroded material. The measured curve definitely shows larger sizes present in the sediment load. This discrepancy may be attributed to inaccuracies in the estimation of sediment entrainment. In the transport capacity formulas an average tractive force concept is implied, which excludes the effect of the large instantaneous fluctuations associated with turbulent tractive forces (Alonso and Coleman, 1981).

Table 1 - Hydraulic conditions in the flume and San Luis Valley Canal studies.

Data Source	Flow Rate (cfs)	Flow Depth (ft)	Average Velocity (fps)	Energy Slope	Manning's Coefficient
Ashida and Michiue (1971) Run 2	1.06	0.22	1.81	0.00440	0.017
Lane and Carlson (1953) Test Section 12	128.0	1.77	4.00	0.00243	0.023

Table 2 - Size distributions used for simulating the flume and San Luis Valley Canal data.

Flume armoring study		San Luis Valley Canal	
Size Class Interval (mm)	Percent per class interval	Size class Interval (mm)	Percent per class interval
0.2 - 0.3	9.5	0.000 - 0.149	4.0
0.3 - 0.4	9.5	0.149 - 0.297	5.7
0.4 - 0.6	11.0	0.297 - 0.590	10.1
0.6 - 0.8	6.0	0.590 - 1.190	12.0
0.8 - 1.0	4.0	1.190 - 2.380	9.2
1.0 - 2.0	12.0	2.380 - 4.760	5.4
2.0 - 4.0	18.0	4.760 - 9.525	13.3
4.0 - 6.0	18.0	9.525 - 19.05	17.9
6.0 - 8.0	10.0	19.05 - 38.10	13.2
8.0 - 10.0	2.0	38.10 - 76.20	9.2

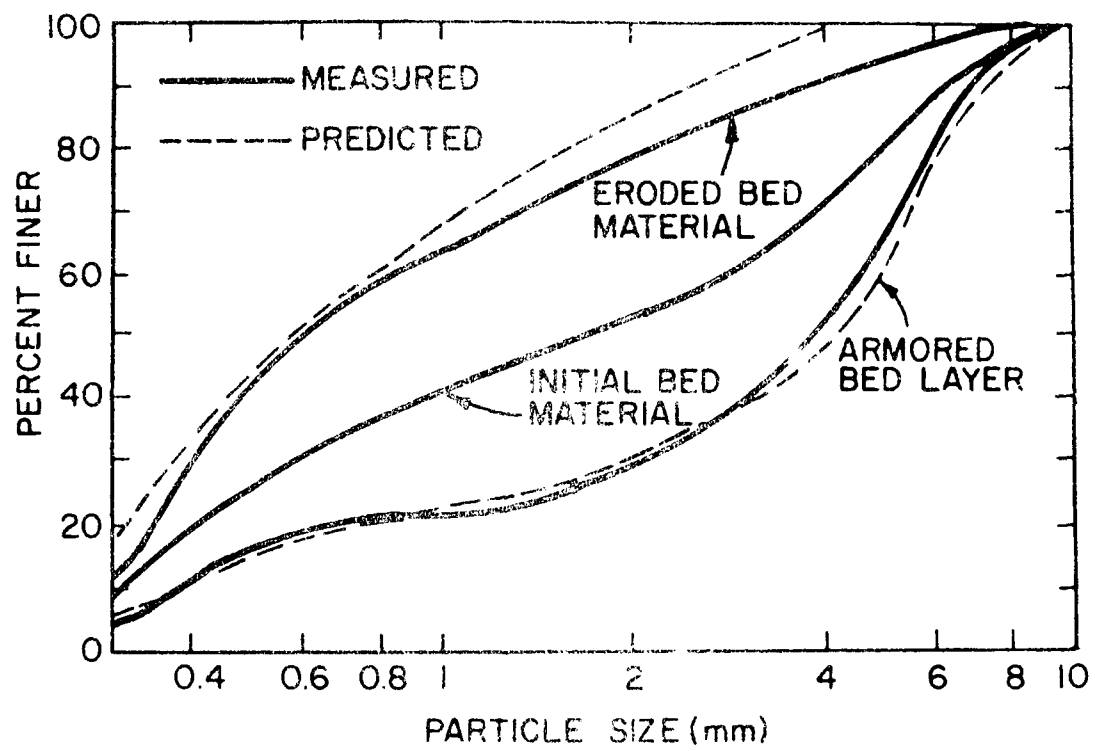


Fig. 12. Size distribution curves obtained for flume armoring test

#### 4.2 SAN LUIS VALLEY CANAL TESTS

The test described in this section is based on data collected by Lane and Carlson (1953) on a reach of one of the canals located in the San Luis Valley of southern Colorado. These canals were constructed in the late 1800's in the alluvial cone deposited by the Rio Grande River on the floor of the San Luis Valley. Near the apex of the cone the deposits consist of sand, gravel, and cobbles, the size of the cobbles decreasing with the distance from the apex. The canals were found very stable, and therefore presented an unusually favorable condition for studies of stable canals. Several reaches ranging in length from 600 to 2200 ft. were selected for study. Hydraulic measurements were made on the most regular portions of the reaches. Observations and mechanical analysis were also made of the bed and bank materials forming the test sections. Samples of the material in which the canal was constructed were obtained by excavating into the bank of each section. Mechanical analysis of the material forming the bed surface layer disclosed that in the stable sections the finer material had been removed from the layer and an armor coat of coarser material was left.

Data from the test section No. 12 was selected to simulate the development of the armor coat. The hydraulic conditions observed in this section are presented in Table 1. The bank and bed material size distributions are shown in Fig. 13. For simulation purposes, a 600 ft. long reach divided into four equal segments was assumed, with a constant inflow of clear water. The initial bed-material size composition, assumed equal to that of the banks, was represented by the distribution listed in Table 2. The size composition of the active layer at 2.5, 12.5, 37.5, and 87.5 hours are shown in Fig. 13. As time increases, the layer is quite rapidly depleted of particles 10 mm in size or smaller, and the distribution in this size range approaches asymptotically the measured curve. However, the simulated distribution in the 10 to 75 mm size range differs from the composition. This difference may be explained in part by the use of a constant rate of discharge. Although information related to the actual history of flows in the canal is not available, Lane and Carlson (1953) mentioned that the canal had sustained flows considerably above those observed during their study. Therefore, the observed bed-layer composition was most probably shaped

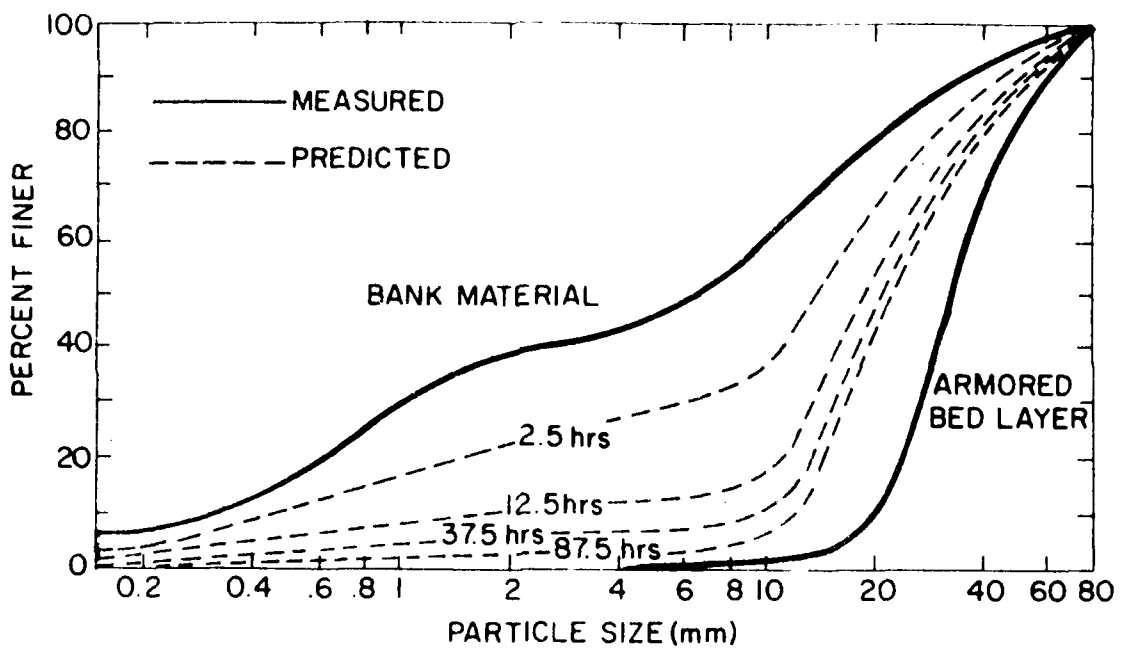


Fig. 13. Evolution of the size distribution in top layer of San Luis Valley Canal.

by flows having transport capacities larger than that used in this simulation. Another reason may be the use of average tractive forces as indicated in the previous section. Nevertheless, there is a clear tendency for the simulated curve to approach the measured size distribution over the entire size range.

#### 4.3 EAST FORK RIVER PROJECT

A detailed program of hydraulic and sediment transport data collection was undertaken by the U.S. Geological Survey during 1975 on a reach of the East Fork River near Boulder, Wyoming. The study reach is approximately 3 miles in length and has a tributary area of about 180 square miles. About half of this area lies within the Wind River Mountains. The other half is provided by the area drained by the Muddy Creek tributary. A map of the study reach showing the position of the principal gaging stations is given in Fig. 14. The river in the study reach is about 60 ft. wide and 4 ft. deep at bank full stage. Most of the water during high flows comes from melting snow of the mountain area. In the East Fork River the bed is gravel on the riffles and bars, but coarse sand constitutes the bulk of the bed load. The bed material in the Muddy Creek is sand but much finer than the sand in the East Fork. Stage recording gages were installed at sections B-1, B-5M, and B-17. Sediment inflow to the reach was measured at sections B-1 and B-5M by sampling suspended sediment with a standard DH-48 hand sampler and determining the bedload discharge with a Helley-Smith bedload sampler. The bedload discharge past the section B-17 was measured with both a bedload trap and a Helley-Smith sampler. Leopold and Emmett (1976) and Mahoney et al. (1976) describe in detail the stream, the bedload trap, and the data collected during 1975. The data included cross-sectional surveys, flow rating curves, water temperature, sediment transport rates, and particle-size distributions of bed load material. This data set was also simulated by Bennett and Nordin (1977). Their input data reduction procedures were followed to some extent in the present test.

In this simulation, the study reach was divided into the fourteen subreaches shown in Fig. 14. Surveys of cross sections were used to obtain relationships between area, wetted perimeter, and stage. Time-averaged active-bed widths were determined from the surveys by comparing

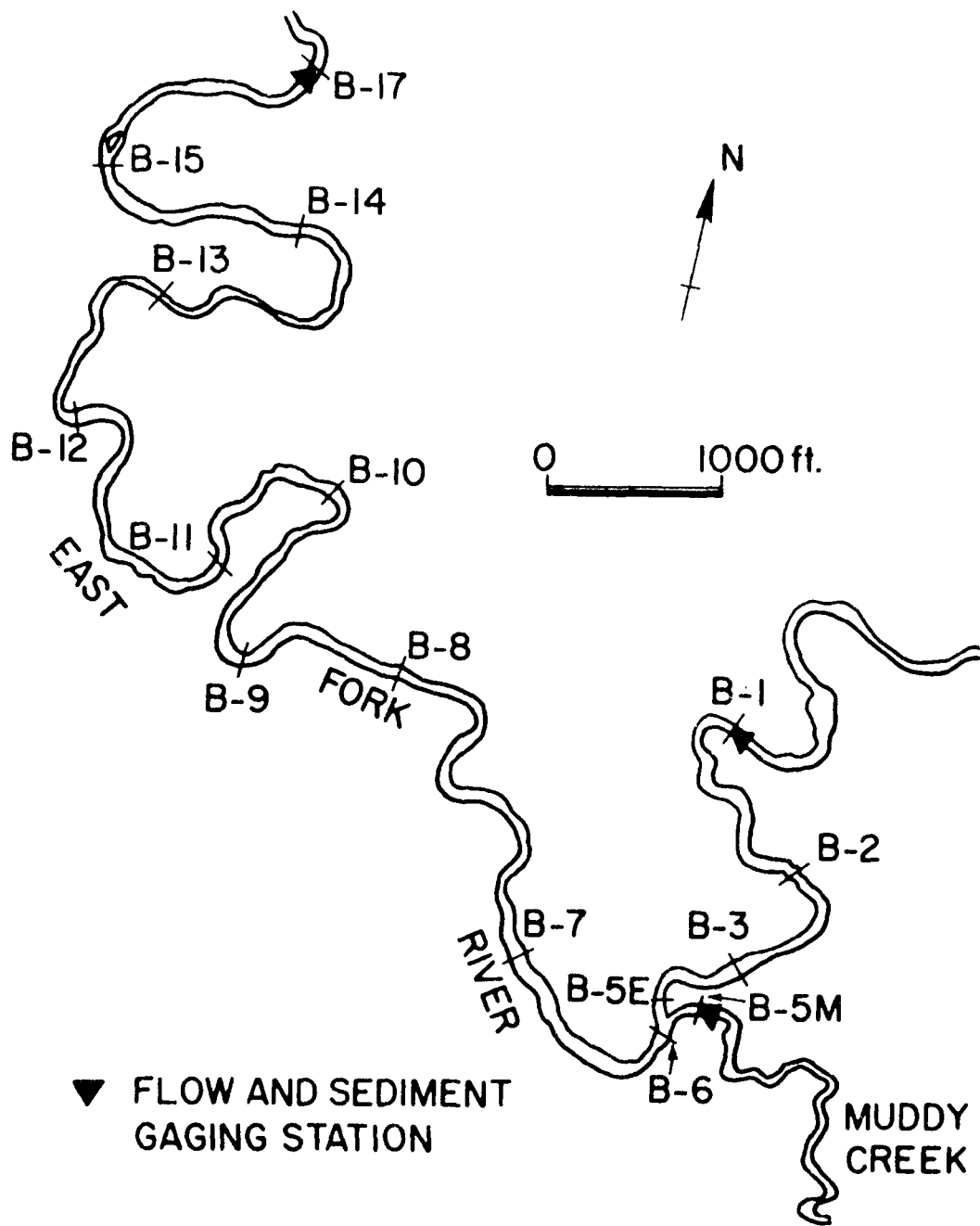


Fig. 14. East Fork River study reach

plots of bed elevation at the beginning and end of the simulation period, and observing which parts of the bed moved vertically. As noted by Bennett and Nordin (1977) this procedure may overestimate the active width because not always all parts of the active width move simultaneously. However, there may be no better way, short of continuous bed monitoring. The profile of six of the cross sections, as measured on June 2, 1975, are plotted in Fig. 15. Also plotted are the estimated active-bed widths, and the stages observed during June 7. As these figures reveal, overbank flow occurred at several sections along the reach during the high flow periods, including the inlet sections B-1 and B-5M.

Flow input to the system was provided by point loads at sections B-1 and B-5M. These point loads were generated by converting the stage readings to flow rates using the rating curves constructed from the stages and flow discharges measured at those sections. The rating curves reported by Mahoney et al. (1976) are shown in Figs. 16a and 16b. The sum of the inflow hydrographs measured during the simulation period is about equal to the outflow hydrograph observed at section B-17, indicating that water was carried by essentially translatory waves. This fact lends further support to the use of a kinematic-wave routing scheme.

Inflow of sediment at sections B-1 and B-5M were obtained from sediment-flow rating curves. These were constructed by relating the measured sediment loads to water discharges obtained from the above flow rating curves. Suspended sediment did not contribute significantly to the total input load and, therefore, the sediment discharges were based solely on the bedload data. When plotted in log-log scales the data exhibited considerable scatter but displayed a linear trend. Linear interpolation of the logarithmic values yielded the rating curves shown in Figs. 16c and 16d. The data scatter resulted in the low correlation coefficients indicated in the figures. A total of ten different fractions with mean diameters 0.12, 0.25, 0.5, 1.0, 2.0, 4.0, 8.0, 16.0, 32.0, and 64.0 mm were selected to represent the sediment in the bed and in transport. The percentages of material associated with each size were determined from the sampled size distributions. These percentages

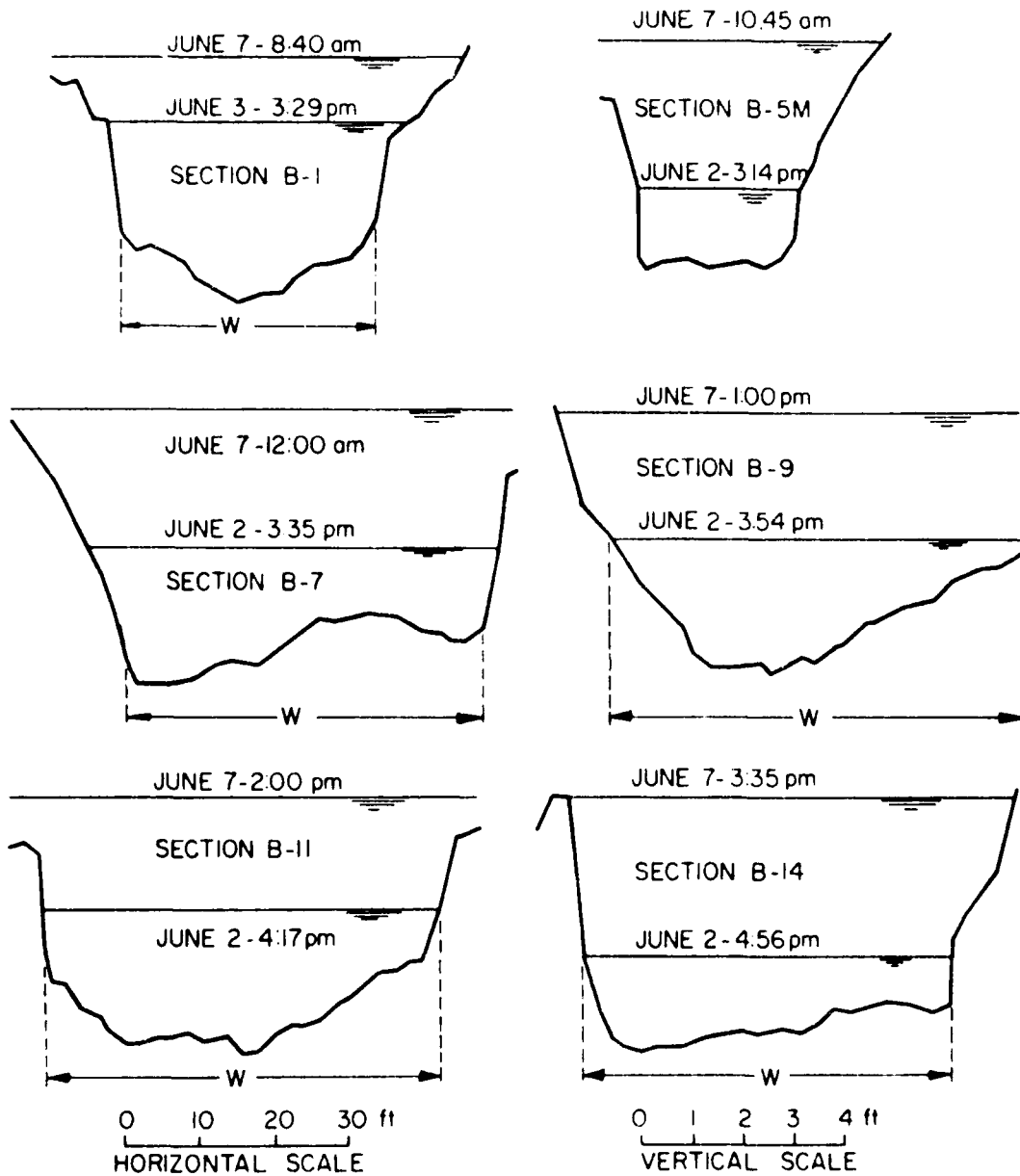


Fig. 15. Examples of reach cross sections. The high and low water stages shown in each cross section were measured in the days and times indicated in the plots.

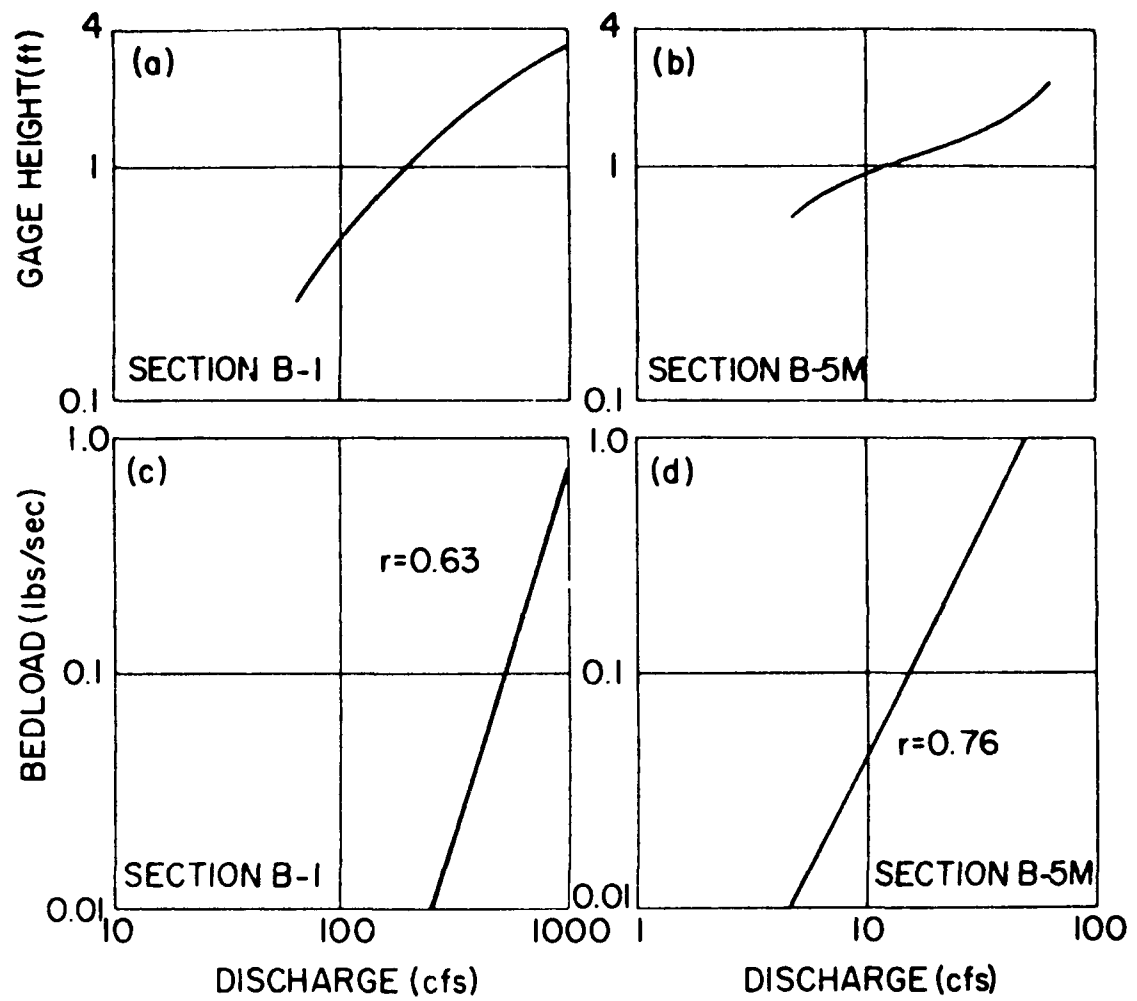


Fig. 16. Flow and sediment rating curves

were used to convert the total bedloads to sediment transport rates for each particle-size fraction. Similar analysis was performed for the data collected at section B-17. These data are used in comparing measured and predicted water and sediment discharge from the study area.

A thirty minute time step was used in modeling the East Fork River for a period of twenty-two days from May 29 through June 19, 1975. The first step involved calibration of the flow parameter to best fit the observed outflow hydrograph. A comparison of simulated and recorded flows at section B-17 is presented in Fig. 17. Agreement is satisfactory at low and intermediate flows, but the measured values exceed the simulated values at high flows. The reason for this discrepancy is the occurrence of overbank flows which were not accounted for in the construction of the flow rating curves (Figs. 16a and 16b).

The next step after obtaining the hydraulic results was simulation of the sediment transport. The simulation was performed a number of times, adjusting each time the sediment parameters to obtain the best possible agreement between simulated and observed values. Fig. 18 shows predicted and recorded bedload discharges at section B-17 for the twenty-two day simulation period. The dashed lines joining the data points are imaginary lines used to approximate the shape of the measured sediment graph. The observed total bedload outflow between June 1 and June 19 is 1889 tons. The predicted value is 1942 tons, less than three percent higher. In spite of this agreement, there is a tendency for the simulated bedload rates to be lower than the recorded values at high flows, and higher during the recessions. The differences are most noticeable during the first high flow period. A possible explanation for these discrepancies is provided by field observation in the East Fork River recently reported by Meade et al. (1981). Over the years they have observed that, during the runoff season, some sections of the reach are scoured while other sections are filled, resulting in a nonuniform storage of movable bed material along the stream. Consequently, the relation of bedload rate to water discharge varies significantly from one part of the reach to another. Meade et al. (1981) noted that immediately downstream of a storage area the bedload

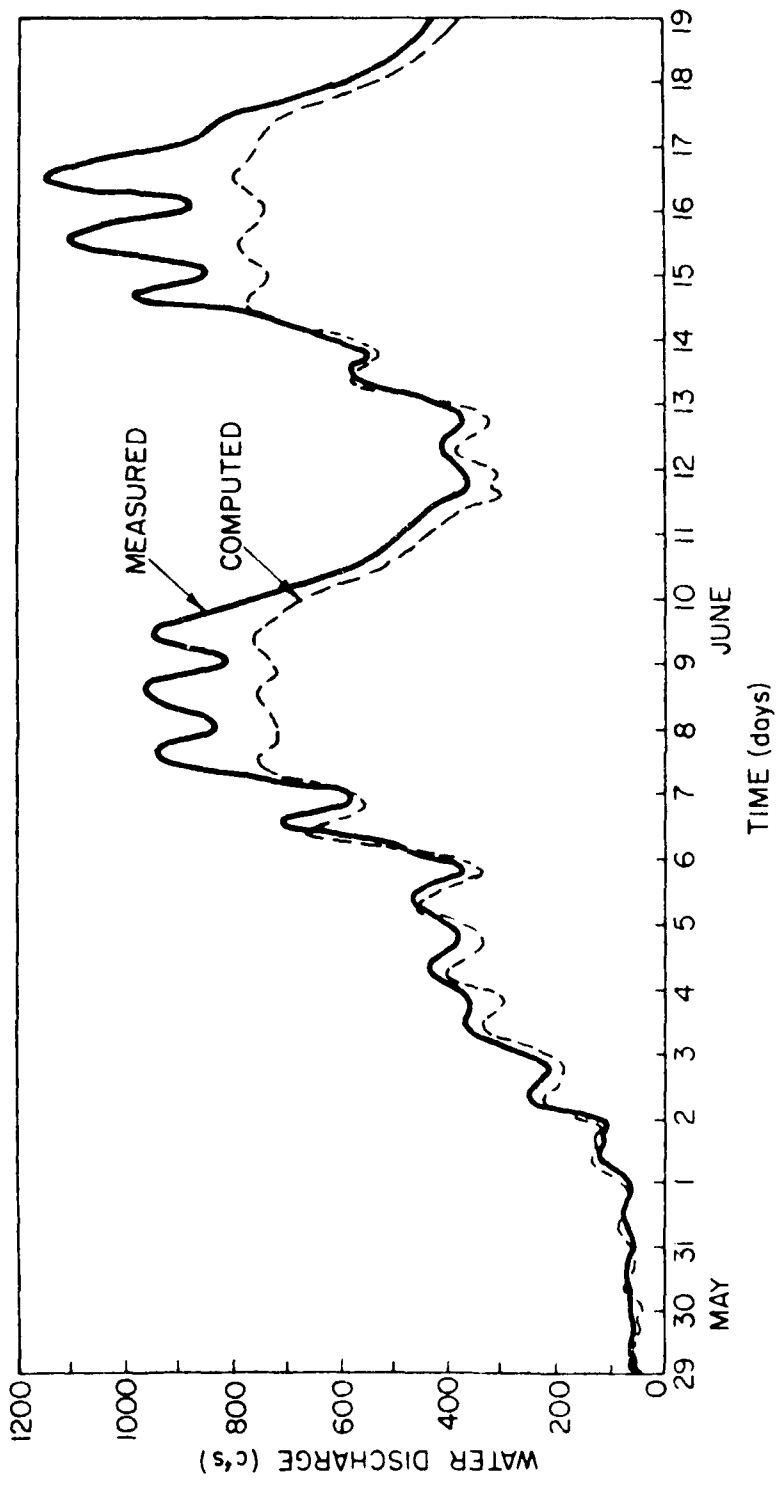


Fig. 17. Measured and predicted flows at station B-17, East Fork River

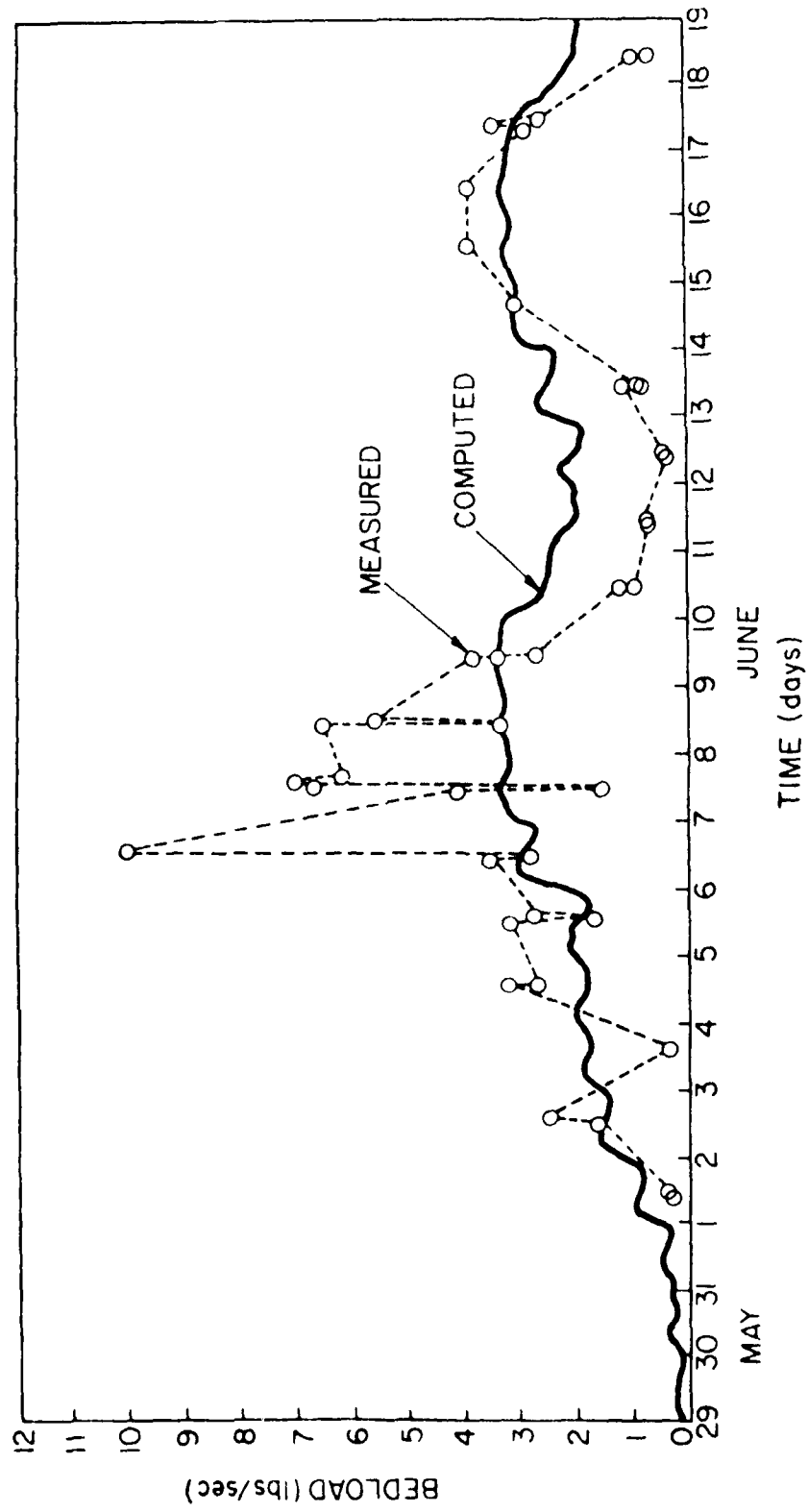


Fig. 18. Measured and predicted bedloads at station B-17, East Fork River

transport may increase steeply with the initial increase in water discharge and later, as the stored movable material becomes depleted the transport rate rapidly decreases, resulting in a multi-valued rating curve. They also mention that this behavior has been indeed observed at the gaging station B-17 (Leopold and Emmett, 1976). This behavior cannot be exactly reproduced by the present model, which assumes a supply of transportable material uniformly distributed along the streambed, and single-valued relations between bedload transport and water discharge at all sections. Nevertheless, the predicted sedimentgraph displays the rising and falling trends observed in the recorded bedload during the twenty-two day time span.

Fig. 19 shows a comparison of simulated against sampled size distribution of the bedload at the beginning, middle, and end of the first high flow period. The model predicts fairly well the distribution of the coarser materials, and the shift of the  $d_{50}$  during the event. The recorded values, however, indicate less mobility of material in the finer size range than predicted. There could be several reasons for this disagreement. For one thing the kinematic-wave approximation used in routing the flow may be distorting the local energy slopes, resulting in overestimation of entrainment threshold conditions. Or, there might have been more fine material being carried in suspension which could not be sampled as part of the bedload, but which was actually accounted for by Yang's total load formula used in the simulation. A definite answer requires further investigation.

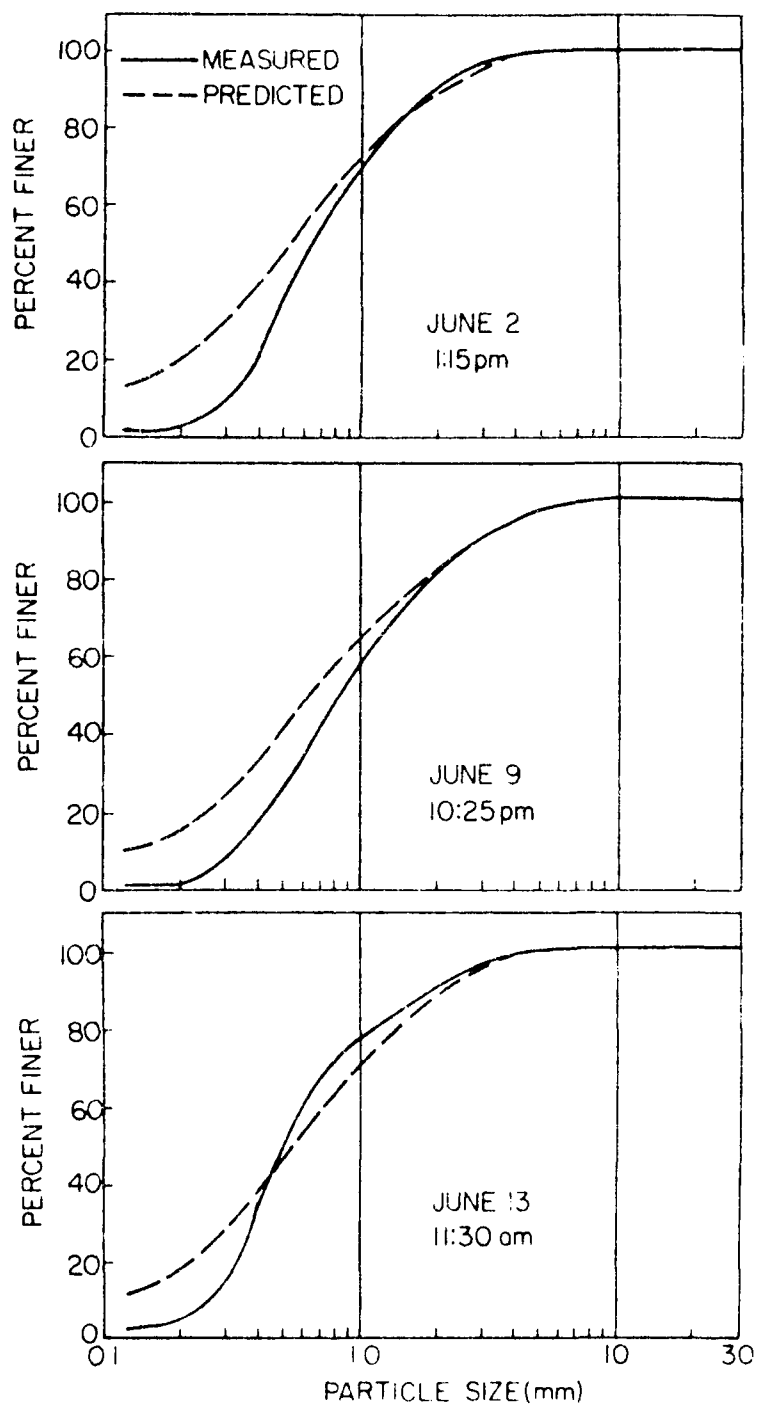


Fig. 19. Measured and predicted bedload size - distributions at station B-17, East Fork River.

## CONCLUSIONS AND RECOMMENDATIONS

## 5.1 CONCLUSIONS

1. A one-dimensional numerical model has been developed for simulating the movement of well graded sediments through a stream network.
2. Hydraulic routing is performed by using any acceptable algorithm supplied by the user because the water movement is assumed uncoupled from the sediment process. The model can be used in conjunction with any suitable sediment yield model to supply the water and sediment runoff from lateral areas.
3. The sediment routing scheme is based on the physical processes governing the mechanics of sediment movement in alluvial channels. The model recognizes the effect of bed and suspended load interaction on the total load movement, can simulate bed armoring, changes in bed elevation, and longitudinal sorting of eroded material.
4. The applicability of the model is restricted to noncohesive materials, relatively stable channel geometries, streams with negligible in and out-of-bank transport, and flows in which transverse currents may be ignored.
5. The model gave satisfactory results when tested on laboratory data from a flume armoring study, and field data from the San Luis Valley Canal, Colorado, and the East Fork River, Wyoming. These tests tend to indicate that the model adequately simulates the transport of graded cohesionless sediments, including the effect of armoring.

## 5.2 RECOMMENDATIONS

1. It is recommended that the channel model be further tested against a variety of real situations with special emphasis on the scour, deposition, and transport of noncohesive materials.
2. It is recommended that the model be further developed and refined to include the following capabilities: (a) improve the one-dimensional representation by separating flows in the incised channel from flows over flood plains; (b) account for in and out-of-bank transport, and lateral distribution of bed-material properties and hydraulic conditions; (c) predict the variation of lateral bed slope and lateral sediment sorting around channel bends; and (d) simulate sediment retention by grasses and other vegetative covers.

3. The channel model should be tested using hypothetical situations to confirm that the model does respond in a realistic manner. For instance, these tests may include the following channel-stability related applications: (a) Consolidate the channel model with continuous sediment yield and bank-stability models. Run the consolidated models for a period of a few years, and predict the size and grade of channel needed to maintain a bank height-slope that is stable for a given stratigraphic condition. (b) Run the consolidated model for a combination of unstable bank and steep grade and observe what combination of bed armoring and/or grade-control structures are predicted to stabilize the channel. (c) Select a range of storm events and use the consolidated model to study slough of bank material, and find channel width and/or armoring coat that is needed to prevent erosion of slough material.
4. It is recommended that data gathering efforts be continued to provide an adequate base for further model development and validation.

#### REFERENCES

1. Alonso, C. V., and Coleman, N. L., "Stochastic properties of turbulent tractive forces in prismatic channels," Appendix J, Final Report to Vicksburg District Corps of Engineers, 1981.
2. Alonso, C. V., Neibling, W. H., and Foster, G. R., "Estimating Sediment Transport Capacity in Watershed Modeling," accepted for publication in the Transactions of the American Society of Agricultural Engineers, 1981.
3. Ashida, K., and Michiue, M., "An Investigation of River Bed Degradation Downstream of a Dam," Proceedings, 14th Congress of the International Association for Hydraulic Research, Vol. 3, 1971, pp. 247-256.
4. Bennett, J. P., and Nordin, C. F., "Simulation of Sediment Transport and Armouring," Hydrological Sciences Bulletin, Vol. XXII, No. 4, 1977, pp. 555-569.
5. Borah, D. K., "Dynamic Simulation of Water and Sediment Movement in Watersheds," Ph.D. dissertation, University of Mississippi, 1979.
6. Borah, D. K., Alonso, C. V., and Prasad, S. N., "A Single-event numerical model for routing water and sediment on small catchments," Appendix I, Final Report to Vicksburg District Corps of Engineers, 1981.
7. Borah, D. K., Prasad, S. N., and Alonso, C. V., "Kinematic Wave Routing Incorporating Shock Fitting," Water Resources Research, Vol. 16, No. 3, 1980, pp. 529-541.
8. Cunge, J. A., and Perdreau, N., "Mobile Bed Fluvial Mathematical Models," La Houille Blanche, No. 7, 1973, pp. 561-580.
9. Einstein, H. A., "The Bed-Load Function for Sediment Transportation in Open Channel Flows," Technical Bulletin No. 1026, USDA, Soil Conservation Service, 1950.
10. Francis, J. R. D., "Experiments on the Motion of Solitary Grains Along the Bed of a Water-Stream," Proceedings, Royal Society of London, Series A, Vol. 332, 1973, pp. 443-471.
11. Gradowczyk, M. H., "Wave Propagation and Boundary Instability in Erodible-Bed Channels," Journal of Fluid Mechanics, Vol. 33, Part 1, 1968, pp. 93-112.

12. Graf, W. H., Hydraulics of Sediment Transport, McGraw-Hill Book Co., New York, 1971.
13. Guy, H. P., "Fluvial Sediment Concepts," Techniques of Water-Resources Investigations of the U.S. Geological Survey, Book 3, Chapter C1, 1970.
14. Jobson, H. E., and Sayre, W. W., "Vertical Transfer in Open Channel Flow," Journal of the Hydraulics Division, ASCE, Vol. 96, No. HY3, 1970, pp. 703-724.
15. Lane, E. W., and Carlson, E. J., "Some Factors Affecting the Stability of Canals Constructed in Coarse Granular Materials," Proceedings, IAHR-ASCE International Hydraulics Convention, Minneapolis, 1953, pp. 37-48.
16. Lean, G. H., "The Settling Velocity of Particles in Channel Flow," in International Symposium on Stochastic Hydraulics, Ed. by C. L. Chiu, University of Pittsburgh, 1971, pp. 339-351.
17. Leopold, L. B., and Emmett, W. W., "Bedload Measurements, East Fork River, Wyoming," Proceedings, The National Academy of Sciences, Washington, Vol. 73, No. 4, 1976, pp. 1000-1004.
18. Mahmood, K., "Mathematical Modeling of Morphological Transients in Sandbed Canals," Proceedings, 16th Congress of the International Association for Hydraulic Research, Vol. 2, 1975, pp. 57-64.
19. Mahoney, H. A., Andrews, E. D., Emmett, W. W., Leopold, L. B., Meade, R. H., Myrick, R. M., and Nordin, C. F., "Data for Calibrating Unsteady - Flow Sediment-Transport Models, East Fork River, Wyoming, 1975," USGS Open-File Report 76-22, 1976.
20. Meade, R. H., Emmett, W. W., and Myrick, R. M., "Movement and Storage of Bed Material During 1979 in East Fork River, Wyoming, USA," to appear in Erosion and Sediment Transport in Pacific Rim Steep Lands, International Association of Hydrological Sciences Publications, 1981.
21. Meyer-Peter, E., and Muller, R., "Formulas for Bed Load Transport," Proceedings, 2nd Congress of the International Association for Hydraulic Research, Stockholm, 1948, pp. 39-64.
22. Miller, W. A., and Yevjevich, V., Ed., Unsteady Flow in Open Channels III: Bibliography, Water Resources Publication, Fort Collins, CO, 1975.

23. Ponce, V. M., Li, R. M., and Simons, D. B., "Applicability of Kinematic and Diffusion Models," Proceedings, 26th ASCE Hydraulics Division Specialty Conference, University of Maryland, August, 1978, pp. 605-613.
24. Ponce, V. M., Lopez Garcia, J., and Simons, D. B., "Modeling Alluvial Channel Bed Transients," Journal of the Hydraulics Division, ASCE, Vol. 105, No. HY3, 1979, pp. 245-256.
25. Thomas, W. A., and Prashun, A. L., "Mathematical Modeling of Scour and Deposition," Journal of the Hydraulics Division, ASCE, Vol. 103, No. HY8, 1977, pp. 851-863.
26. Vanoni, V. A., Ed., Sedimentation Engineering, American Society of Civil Engineers, New York, 1975.
27. Vries, M. de, "Solving River Problems by Hydraulic and Mathematical Models," Publication No. 76 II, Delft Hydraulics Laboratory, 1971.
28. Whitham, G. B., Linear and Nonlinear Waves, John Wiley, New York, 1974.
29. Yang, C. T., "Incipient Motion and Sediment Transport," Journal of the Hydraulics Division, ASCE, Vol. 99, No. HY10, 1973, pp. 1679-1704.

#### ADDENDUM 1: SEDIMENT CONTINUITY EQUATION

Consider an unsteady streamflow carrying sediment down a channel with arbitrary cross-sectional geometry and alignment (Fig. 1.1). The volume concentration of the sediment-laden flow,  $c$ , may vary from point to point, and as a result of convection, from instant to instant at any point. The lateral volume rate of sediment inflow,  $q_\ell$ , can vary with both space and time. The continuity equation for an infinitesimal unit volume in the neighborhood of a fixed point is

$$\frac{\partial c}{\partial t} + \frac{\partial c u_k}{\partial x_k} = 0, \quad (1.1)$$

in which  $u_k$  is the instantaneous local velocity component of the sediment-laden fluid along the  $x_k$ -direction. Repetition of the subscript  $k$  in a term implies summation over the three orthogonal coordinate directions. In a turbulent flow, time averaging Eq. 1.1 yields

$$\bar{\frac{\partial c}{\partial t}} + \bar{\frac{\partial}{\partial x_k}} (\bar{c} \bar{u}_k + \bar{c}' \bar{u}'_k) = 0, \quad (1.2)$$

where the overbars indicate temporal means, and the primed terms represent turbulent fluctuations. Let assume the mean cross sectional area,  $\bar{A}$ , of the channel divided in two parts. One part,  $\bar{A}_1$ , is occupied by the sediment carried in suspension, and another,  $\bar{A}_2$ , is occupied by the sediment transported as bedload. It should be noted herein that the orientation of the coordinate system is arbitrary and, in general,  $\bar{A}$  is a function of  $x_k$  as well as of time. For convenience, the coordinate system will be chosen so that the direction normal to  $\bar{A}$  coincides with the streamwise direction  $x$  (Fig. 1.1). The continuity equation for the suspended-load section is obtained by integrating Eq. 1.2 over  $\bar{A}_1$ , to obtain

$$\iint_{\bar{A}_1} \bar{\frac{\partial c}{\partial t}} d\bar{A}_1 + \iint_{\bar{A}_1} \bar{\frac{\partial}{\partial x}} (\bar{c}_1 \bar{u}_1 + \bar{c}'_1 \bar{u}'_1) d\bar{A}_1 = 0. \quad (1.3)$$

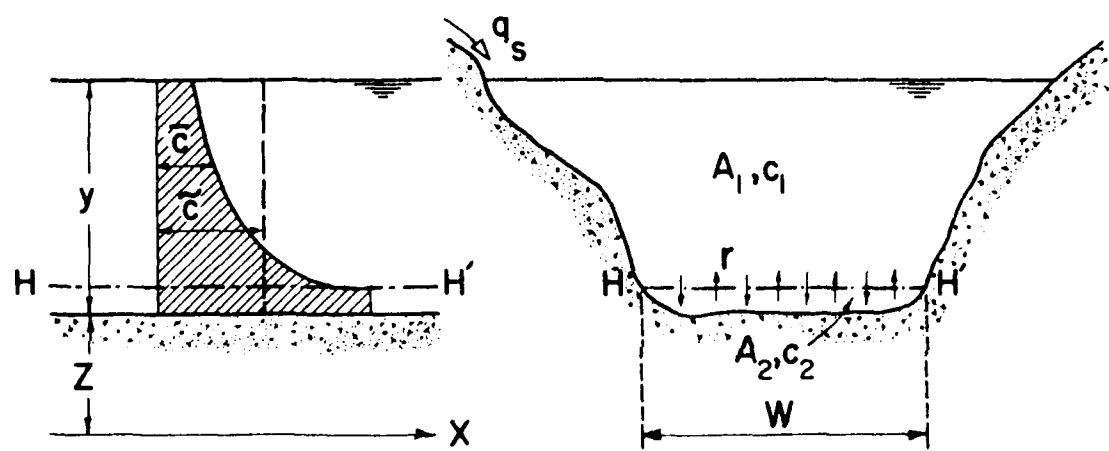


Fig. 1-1 - Definition sketch of vertical transfer.

Using Leibnitz's rule:

$$\begin{aligned} \frac{\partial}{\partial t} \iint_{\bar{A}_1} \bar{c}_1 d\bar{A}_1 &= [\bar{c}_1 - \frac{\partial \bar{A}_1}{\partial t}]_{\bar{\sigma}_1} + \frac{\partial}{\partial x} \iint_{\bar{A}_1} (\bar{c}_1 \bar{u} + \bar{c}'_1 \bar{u}') d\bar{A}_1 = \\ &= [(\bar{c}_1 \bar{u} + \bar{c}'_1 \bar{u}')] \frac{\partial \bar{A}_1}{\partial x} \Big|_{\bar{\sigma}_1} = 0, \end{aligned} \quad (1.4)$$

in which  $\bar{\sigma}_1$  is the mean perimeter bounding the mean area  $\bar{A}_1$ . The boundary condition for this cross section is

$$[\bar{c}_1 \frac{d\bar{A}_1}{dt}]_{\bar{\sigma}_1} = [\bar{c}_1 (\frac{\partial \bar{A}_1}{\partial t} + u \frac{\partial \bar{A}_1}{\partial x})]_{\bar{\sigma}_1} = \int_{\bar{\sigma}_1} \bar{c}_1 q_\ell d\bar{\sigma}_1, \quad (1.5)$$

where  $q_\ell$ , the volume rate of lateral sediment inflow per unit length of  $\bar{\sigma}_1$ , is taken positive for inflow. Expanding Eq. 1.5 and time averaging gives

$$[\bar{c}_1 \frac{\partial \bar{A}_1}{\partial t} + \bar{c}_1 \bar{u} \frac{\partial \bar{A}_1}{\partial x} + \bar{c}'_1 \bar{u}'] \frac{\partial \bar{A}_1}{\partial x} \Big|_{\bar{\sigma}_1} = \int_{\bar{\sigma}_1} (\bar{c}_1 \bar{q}_\ell + \bar{c}'_1 \bar{q}'_\ell) d\bar{\sigma}_1. \quad (1.6)$$

Substituting this equation into Eq. 1.4 yields

$$\frac{\partial}{\partial t} \iint_{\bar{A}_1} \bar{c}_1 d\bar{A}_1 + \frac{\partial}{\partial x} \iint_{\bar{A}_1} (\bar{c}_1 \bar{u} + \bar{c}'_1 \bar{u}') d\bar{A}_1 = \int_{\bar{\sigma}_1} (\bar{c}_1 \bar{q}_\ell + \bar{c}'_1 \bar{q}'_\ell) d\bar{\sigma}_1 \quad (1.7)$$

Analogous to the Reynolds closure scheme for turbulent momentum transfer, an eddy mass diffusivity tensor,  $\varepsilon$ , is introduced such that

$$\bar{c}'_1 \bar{u}' = -\varepsilon \frac{\partial \bar{c}_1}{\partial x} \quad (1.8)$$

Now let

$$\bar{c}_1 = \tilde{c}_1 + c_1^*, \quad (1.9)$$

and

$$\tilde{u} = \hat{u} + u^*, \quad (1.10)$$

where the tildes denote spatial averages over  $\bar{A}_1$ , and the asterisks denote deviation from the spatial averages. Substitution of Eqs. 1.8, 1.9, and 1.10 into Eq. 1.7 gives

$$\begin{aligned} \frac{\partial \bar{A}_1 \tilde{c}_1}{\partial t} + \frac{\partial Q_1}{\partial x} &= \frac{\partial}{\partial x} \iint_{\bar{A}_1} (\varepsilon \frac{\partial \bar{c}_1}{\partial x} - c_1^* u^*) d\bar{A}_1 + \\ &\quad \int_{\bar{\sigma}_1} (\bar{c}_1 \bar{q}_\ell + \bar{c}_1' \bar{q}_\ell') d\bar{\sigma}_1, \end{aligned} \quad (1.11)$$

where

$$Q_1 = \iint_{\bar{A}_1} \tilde{c}_1 \tilde{u} d\bar{A}_1$$

represents the volume rate of suspended sediment discharge. The first integral on the right hand side of Eq. 1.11 denotes the rate of longitudinal dispersion of sediment. The second integral can be replaced by the sum of the sediment inflow from runoff and tributaries,  $q_s$ , and the rate of sediment volume transfer across H-H' (Fig. 1.1) from the bedload zone, denoted herein as  $-\partial r_1 / \partial t$ . Longitudinal dispersion in the suspended zone is negligible with respect to vertical dispersion and can be omitted. Thus, Eq. 1.11 becomes

$$\frac{\partial \bar{A}_1 \tilde{c}_1}{\partial t} + \frac{\partial Q_1}{\partial x} = q_s - \frac{\partial r_1}{\partial t} \quad (1.12)$$

Similarly, integrating Eq. 1.2 over  $\bar{A}_2$  yields the continuity equation for the bedload,

$$\frac{\partial \bar{A}_2 \tilde{c}_2}{\partial t} + \frac{\partial Q_2}{\partial x} = \int_{\bar{\sigma}_2} (\bar{c}_2 \bar{q}_\ell + \bar{c}_2' \bar{q}_\ell') d\bar{\sigma}_2, \quad (1.13)$$

where  $Q_2$  is the volume rate of bedload discharge, and  $\bar{\sigma}_2$  is the mean perimeter bounding  $\bar{A}_2$ . Two different sources contribute to the integral in the right hand side of Eq. 1.13. One is the rate of sediment volume transfer across H-H' from the suspended zone, and denoted  $\partial r_2 / \partial t$ . The other contribution comes from the rate of sediment exchange with the bed surface, which can be approximated by

$$q_b = -(1-\lambda)W \frac{\partial z}{\partial t}, \quad (1.14)$$

where  $\lambda$  is the bed porosity,  $W$  defines the active bed width (Fig. 1.1), and  $z$  is the local bed elevation above a reference datum. The negative sign in Eq. 1.14 accounts for the fact that the sediment flux across  $\bar{\sigma}_2$  is negative when sediment settles out of the bedload zone during bed aggradation ( $\partial z / \partial t > 0$ ). Replacing the integral in Eq. 1.13 by the sum of  $\partial r_2 / \partial t$  and  $q_b$  gives

$$\frac{\partial \bar{A}_2 \tilde{c}_2}{\partial t} + \frac{\partial Q_2}{\partial x} = \frac{\partial r_2}{\partial t} - (1-\lambda)W \frac{\partial z}{\partial t} \quad (1.15)$$

Adding Eqs. 1.12 and 1.15 results in

$$\frac{\partial \bar{A} \tilde{c}}{\partial t} + \frac{\partial Q_s}{\partial x} + (1-\lambda)W \frac{\partial z}{\partial t} + \left[ \frac{\partial r_1}{\partial t} - \frac{\partial r_2}{\partial t} \right] = q_s, \quad (1.16)$$

where  $\bar{A} \tilde{c} = \bar{A}_1 \tilde{c}_1 + \bar{A}_2 \tilde{c}_2$ , and  $Q_s = Q_1 + Q_2$ . The term within brackets represents the net rate of sediment volume transfer across H-H'. This term is different from zero whenever a net amount of sediment passes from the bedload to the suspended load zone, or vice versa, as a result of bed scour or sediment deposition. Letting

$$\frac{\partial r}{\partial t} = \frac{\partial r_1}{\partial t} - \frac{\partial r_2}{\partial t},$$

and dropping the tildes and overbars, Eq. 1.16 becomes

$$\frac{\partial A c}{\partial t} + \frac{\partial Q_s}{\partial x} + (1-\lambda) W \frac{\partial z}{\partial t} + \frac{\partial r}{\partial t} = q_s, \quad (1.17)$$

in which  $Q_s$  is the total volume sediment discharge, and  $c$  is the total average volume concentration. Eq. 1.17 is the sediment continuity equation used in the present model, and equally applies to streamflows carrying sediment mostly in suspension or as bedload.

## ADDENDUM 2: SUMMARY OF TRANSPORT FORMULAS

This Addendum describes briefly the transport formulas used in the present model. Each formula is presented as the originator intended, but rewritten in terms of dimensionless parameters. Where the formulations required graphical solutions (i.e., determination of threshold conditions from Shield's curve), analytical equivalents (not shown here) have been worked out to facilitate their use in digital computation.

Total load formula of Yang (1973):

$$\Phi = \theta_{50}^{1/2} Z_{50} (V/u_*^*) [10^{\phi - 6}/S], \quad (2.1)$$

where

$$\begin{aligned} \phi = & 5.435 - 0.286 \log (w d_{50}/v) - 0.457 \log (u_*^*/w) + \\ & [1.799 - 0.409 \log (w d_{50}/v) - 0.314 \log (u_*^*/w)] \\ & \log (VS_0/w - V_c S_0/w), \end{aligned} \quad (2.2)$$

$$\frac{V_c}{w} = \begin{cases} 2.5 / [\log(u_*^* d_{50}/v) - 0.06] + 0.66, & 0 < u_*^* d_{50}/v < 70, \\ 2.05, & u_*^* d_{50}/v \geq 70. \end{cases} \quad (2.3)$$

DuBoys-type bedload formula (Graft, 1971):

$$\Phi = \sigma \theta^2 (1 - \theta/\theta_c) \quad (2.5)$$

where

$$\sigma = \chi (S-1)^{3/2} \rho^2 g^{3/2} d^{1/2}. \quad (2.6)$$

Empirical relationships for the sediment coefficient  $\chi$  are given by Graft (1971).

Bedload formula of Meyer-Peter and Muller (1948):

$$\Phi = 8 \theta_{50}^{3/2} [K^{3/2} - \theta_c/\theta_m]^{3/2}, \quad (2.7)$$

in which

$$K = (V/u_*) (f_b/8)^{1/2} \quad (2.8)$$

The friction factor associated with bed skin friction,  $f_b$ , is obtained from (Vanoni, 1975)

$$(f_b)^{-\frac{1}{2}} + 2 \log (k_s / 4 R_b) = 1.14 - \\ 2 \log [1 + \frac{37.40 R_b}{k_s N_R (f_b)^{\frac{1}{2}}}], \quad 3 < \frac{u_* k_s}{v} \leq 70, \quad (2.9)$$

$$(f_b)^{-\frac{1}{2}} = 2 \log (4 R_b / k_s) + 1.14, \quad \frac{u_* k_s}{v} > 70, \quad (2.10)$$

where  $k_s = d_{90}$ ,  $N_R$  is the flow Reynolds number, and  $R_b$  is the bed hydraulic radius.

In Eqs. 2.1, 2.5, and 2.7  $\phi$  is the dimensionless volume transport rate,  $\theta_k$  and  $Z_k$  are the mobility number and relative roughness based on the  $d_k$  grain size, and the subscript c denotes threshold conditions. These parameters are defined as

$$\phi = (Q_s/W)/[(S-1)gd_{50}^3]^{\frac{1}{2}}, \quad (2.11)$$

$$\theta_k = u_*^2 / [(S-1)gd_k], \quad (2.12)$$

and

$$Z_k = y/d_k, \quad (2.13)$$

where S is the specific gravity of the bed material, and  $u_*$  is the bed shear velocity.

### ADDENDUM 3: DESCRIPTION OF COMPUTER PROGRAM

The computer program used in the simulation of the East Fork River data is listed below. The program consists of a main program and several subroutines. The main program inputs the required data to the system, calls the subroutines according to the computational scheme, and prints out the calculated results. Subroutine WROUT is a user supplied program that routes water through a channel reach for each time step. Subroutine SROUT performs sediment routing through a reach for each time step, and it calls in turn subroutines DUBOYS, MEYER, SETVEL, SHIELD, and YANG. These subroutines compute potential carrying capacities and sediment transport parameters.

In order to minimize the need for core memory, the program was organized by taking advantage of the absence of backwater conditions in the present simulations. In the adopted organization the length of the entire channel reach is divided into a few segments, or channel blocks, and the time steps used for the whole simulation period are grouped into several consecutive time blocks. Then, the channel blocks are processed in sequence for each time block. Input data for each channel and time block are stored in disk files. A list of the important variables in the computer program is given in the following section.

The codes requires 72,741 words on a Mod Comp Classic computer system. This is a 16-bit machine that uses two words for each single precision variable. The execution time for the East Fork River test is approximately 9 minutes.

#### List of Fortran Variables

<u>Name</u>	<u>Description</u>	<u>Units</u>
ACCM(IF, IFA)	Element of volume entrainment matrix at the start of the current time step. IFA indicates the material fraction exposed by the removal of fraction IF.	ft <sup>3</sup>
AE	Area of flow cross section at the start of the current time step.	ft <sup>2</sup>

ARMHT	Current thickness of active layer.	ft
BEDELV(IC)	Bed elevation of section IC at the end of the current time step.	ft
BEDMAT(IF)	Vector used to store the volume of individual material fractions present in the bed layer.	ft <sup>3</sup>
BEDUP	Change in bed elevation caused by deposition during the current time step.	ft
BEDWN	Change in bed elevation caused by erosion during the current time step.	ft
CAP	Volume concentration of individual material fractions at transport capacity.	ft <sup>3</sup> /ft <sup>3</sup>
CC(IC, IF)	Volume concentration of material fraction IF passing through the section IC at the end of the current time step.	ft <sup>3</sup> /ft <sup>3</sup>
CDEP(IC)	Coefficient of power formula relating area of cross-section IC to water depth.	-
CHEZY	Chezy's roughness coefficient.	ft <sup>1/2</sup> /sec
CHI	Coefficient for the DuBoys sediment transport formula.	ft <sup>5.25</sup> /lb <sup>2</sup> .sec
CI(IC, IF)	Volume concentration of material fraction IF passing through the section IC at the start of the current time step.	ft <sup>3</sup> /ft <sup>3</sup>

COEF(J)	Coefficient of the entrainment frequency matrix.	-
CONC	Capacity concentration predicted by transport formulas.	ppm
CPER(IC)	Coefficient of power formula relating wetted perimeter of section IC to flow cross-sectional area.	-
CUP(1T, IF)	Volume concentration of inflow of material fraction IF at the start of the current time step.	ft <sup>3</sup> /ft <sup>3</sup>
DARM	Size of smallest bed material fraction that becomes immobile in the active layer.	mm
DELT	Time taken by a sediment characteristic to travel the distance DELX.	sec
DELX	Channel length increment used in the computational grid.	ft
DEPO	Volume of fraction IF deposited on the bed during the current time step.	ft <sup>3</sup>
DMM(IF)	Representative size of sediment fraction IF.	mm
DPTH	Water depth.	ft
DTS	Size of current time step.	sec
EDEP(IC)	Exponent of power formula relating area of cross-section IC to water depth.	-

EPER(IC)	Exponent of power formula relating wetted perimeter of cross-section IC to flow cross-sectional area.	-
ERS(IF)	Volume of sediment fraction IF eroded from the bed during the current time step.	ft <sup>3</sup>
ERO	Parameter controlling detachment of bed material.	-
G(IT, I, IF)	Calculated volume discharge of sedi- ment fraction IF passing through the downstream end of channel block I, at the end of the current time step IT.	ft <sup>3</sup> /sec
GAMA	Specific weight of water.	lbs/ft <sup>3</sup>
GMES(IT, I, IF)	Measured inflow of sediment fraction IF to channel block I, at the start of the current time step IT.	lbs/sec
GTOTC(IT)	Calculated sediment discharge passing through the channel outlet at the end of the current time step IT.	lbs/sec
GTOTM(IT)	Measured sediment discharge passing through the channel outlet at the start of the current time step IT.	lbs/sec
I	Index identifying channel block.	-
IF	Index identifying sediment-size fraction.	-
INLS	Number of channel subbreaches in a channel block.	-

IT	Computation time step.	-
ITCOM	Number of time steps in simulation period.	-
KIN	Kinematic-wave routing parameter.	-
GLAT(IT)	Lateral volume inflow of sediment to channel block, during the current time step IT.	ft <sup>3</sup> /sec
MEYERP	Coefficient in the Meyer-Peter and Muller sediment transport formula.	-
N	Number of time blocks the simulation period is divided into.	-
NARM	Integer identifying the smallest size fraction that becomes immobile in the active layer.	-
NFR	Number of representative size fractions used in the simulation.	-
NSEG	Number of channel blocks.	-
PCBC(IC, IF)	Percentage of material fraction IF present in the active bed layer of cross section IC.	-
PCF(IC, IF)	Percent of material finer than size IF present in the active bed layer of cross section IC.	-
PCFF(I, IC, IF)	Initial percent of material finer than size IF present in the active bed layer of cross section IC in the channel block I.	-

PCW(IF)	Percent of material in transport finer than size IF passing through the channel outlet.	-
POR(IF)	Porosity of bed material fraction IF.	$\text{ft}^3/\text{ft}^3$
Q(IT)	Computed water discharge at the end of the channel block I, and at the end of the current time step IT.	$\text{ft}^3/\text{sec}$
QLAT(IT)	Lateral water inflow to channel block, during the current time step IT.	$\text{ft}^3/\text{sec}$
QMES(IT, I)	Measured water inflow to channel block I, at the start of the current time step IT.	$\text{ft}^3/\text{sec}$
QUP(IT)	Upstream water inflow to channel block, at the start of the current time step IT.	$\text{ft}^3/\text{sec}$
RESCAP	Residual transport capacity of an individual material fraction, expressed as volume of dry sediment per unit length of channel.	$\text{ft}^3/\text{ft}$
RHB	Hydraulic radius.	ft
SCAP(IF)	Potential transport capacity of material fraction IF, expressed as volume of dry sediment per unit length of channel.	$\text{ft}^3/\text{ft}$
SLN	Length of channel block.	ft
SLOPE(IC)	Channel bed slope at section IC.	$\text{ft}/\text{ft}$

SNU	Average value of the kinematic viscosity of water for the simulation period.	ft <sup>2</sup> /sec
SPGR	Specific gravity of sediment material.	-
SUM	Summation term in Eq. 11.	-
TAO	Average unit tractive force.	lbs/ft <sup>2</sup>
TBM	Total volume of bed material contained in the active layer per unit length of channel.	ft <sup>3</sup>
TC	Critical unit tractive force.	lbs/ft <sup>2</sup>
TCA(IF)	Sum of all the elements in row IF of the volume entrainment matrix.	ft <sup>3</sup>
TEMP	Average water temperature for the simulation period.	Fahrenheit
TGIN(IF)	Vector used to store the measured volumes of all fractions that enter the channel during the simulation period.	ft <sup>3</sup>
TGM(IF)	Vector used to store the measured volumes of all fractions that leave the channel during the simulation period.	ft <sup>3</sup>
TGMES	Total sediment yield measured at the channel outlet.	lbs
TGO(IF)	Vector used to store the computed yield of individual fractions.	lbs

TGOUT	Total sediment yield computed at the channel outlet.	lbs
UST	Bed shear velocity.	ft/sec
VEL	Average velocity of flow.	ft/sec
VS(IF)	Settling velocity in quiescent water for material fraction IF.	ft/sec
WATMAT(IF)	Vector used to store the volumes of all the material fractions being carried by the flow during the current time step.	ft <sup>3</sup>
WEP	Wetted perimeter of channel cross section.	ft
WIDTH(IC)	Vector used to store the active bed width of all channel cross sections.	ft
XSI(IC)	Distance of cross-section IC to upstream boundary of channel block containing IC.	ft

```

C   LIST OF COMPUTER PROGRAM USED IN THE EAST FORK RIVER TEST
C ****
C
C   DIMENSION TITLE(20),QMFS(264,3),QOUT(300),GMES(264,10,3),
&PCFF(3,6,10),PCF(21,10),PCFR(21,10),GTOTM(264),CTOTC(264),
&QS(21),INT(21),GS(21),CII(3,6,10),BEDLVL(3,6),TGO(10),TGM(10),
&TGIN(10)
C   COMMON /ROUT/ I,IT,SLN,CHEZY,DTS,ITCOM,INL,QBASE,
&QUP(300),QI(50,2),XI(50),KSI(50),Q(300,3)
C   COMMON /WROUT/ SLOP,QLAT(300),QC(50,2),XC(50),KSC(50)
C   COMMON /SRROUT/ SPGR,GAMA,SNU,NFR,INLS,WIDTH(10),SLOPE(10),
&CPER(10),EPER(10),CDEP(10),EDEP(10),GLAT(300,10),XSI(10),
&XSC(10,10),REDELV(10),CI(10,10),CC(10,10),PCRI(10,10),PCBC(10,10),
&CUP(300,10),DMM(10),COEF(10),VS(10),POR(10),G(264,3,10),PCW(10),
&ERO,CHI,CEL
C
C   DATA INPUT
C   GENERAL INFORMATION
    READ(4,406) NSEG,DTS,ITCOM,NFR
C   PHYSICAL PROPERTIES
    READ(4,407) TEMP,GAMA,SPGR,SNU
    READ(4,408) (DMM(IF),IF=1,NFR)
C   WATER AND SEDIMENT ROUTING PARAMETERS
    READ(4,409) ERO,CHI,CEL,CHEZY
C   INITIAL BED MATERIAL SIZE DISTRIBUTION
    READ(4,405) ((PCFF(1,IC,IF),IF=1,10),IC=1,3)
    READ(4,405) ((PCFF(2,IC,IF),IF=1,10),IC=1,4)
    READ(4,405) ((PCFF(3,IC,IF),IF=1,10),IC=1,6)
C   COEFFICIENTS OF ENTRAINMENT FREQUENCY MATRIX
    COEF(1)=1.0
    COEF(2)=1.0
    DO 280 J=3,NFR
280   COEF(J)=2.0*COEF(J-1)
    SUBW=(SPGR-1.0)*GAMA
C   POROSITY AND SETTLING VELOCITY
    DO 88 I=1,NFR
      POR(I)=1.-0.245-0.0864/(0.1*DMM(I))**0.21
      D=DMM(I)
      CALL SETVEL(D,W)
      VS(I)=W/30.48
88   CONTINUE
C
C   BEGINNING OF TIME-BLOCK LOOP
    DO 999 N=1,4
C   MEASURED WATER DISCHARGE AT SECTIONS B-1, B-5M, AND B-17
    DO 351 I=1,3
      READ(3,333) (QMES(IT,I),IT=1,ITCOM)
351   CONTINUE
C   MEASURED SEDIMENT DISCHARGE AT SECTIONS B-1, B-5M, AND B-17
    DO 350 I1=1,3
    DO 888 IT=1,ITCOM
      QLOG=ALOG10(QMES(IT,I1))
      IF(I1.EQ.1) EXPONT=3.05785*QLOG-9.33462
      IF(I1.EQ.2) EXPONT=1.92638*QLOG-3.29409
      IF(I1.EQ.3) EXPONT=1.96664*QLOG-5.03781
      GTOTM(IT)=10.0**EXPONT
888   CONTINUE
    READ(4,401) NINT
    WRITE(5,401) NINT
    READ(4,402) (INT(I),QS(I),GS(I),(PCF(I,J),J=1,NFR),I=1,NINT)

```

```

      WRITE(5,402) (INT(I),QS(I),GS(I),(PCF(I,J),J=1,NFR),I=1,NINT)
      I2=I1
      DO 309 I=1,NINT
      PCP=0.0
      DO 301 J=1,NFR
      PC=PCF(I,J)-PCP
      PCFR(I,J)=PC/100.0
      PCP=PCF(I,J)
301   CONTINUE
309   CONTINUE
      DO 302 IF=1,NFR
      DO 303 I=1,NINT
      IF(I.GT.1) GO TO 304
      INT1=INT(I)
      DO 305 J=1,INT1
305   GMES(J,IF,I1)=PCFR(1,IF)*GTOTM(J)
      KC=INT(I)
      GO TO 303
304   IF(I.EQ.NINT) GO TO 306
      IB=KC+1
      IE=INT(I)
      GD=(PCFR(I,IF)-PCFR(I-1,IF))/FLOAT(IE-KC)
      DO 307 J=IB,IE
307   GMES(J,IF,I1)=(PCFR(I-1,IF)+GD*FLOAT(J-KC))*GTOTM(J)
      KC=INT(I)
      GO TO 303
306   CONTINUE
      INT2=INT(NINT)
      DO 308 J=INT2,ITCOM
308   GMES(J,IF,I1)=PCFR(NINT,IF)*GTOTM(J)
303   CONTINUE
302   CONTINUE
350   CONTINUE
C
C BEGINNING OF CHANNEL-BLOCK LOOP
      DO 201 I=1,NSEG
      INL=40
      READ(1,403) INLS,SLN
      WRITE(5,403) INLS,SLN
C GEOMETRIC INPUT FOR CHANNEL BLOCK
      READ(1,404) (XSI(IC),SLOPE(IC),WIDTH(IC),CPER(IC),EPPER(IC),
      &CDEP(IC),EDEP(IC),IC=1,INLS)
      WRITE(5,404) (XSI(IC),SLOPE(IC),WIDTH(IC),CPER(IC),EPPER(IC),
      &CDEP(IC),EDEP(IC),IC=1,INLS)
      DO 801 IC=1,INLS
      PCP=0.0
      DO 802 IF=1,NFR
      PCF(IC,IF)=PCFF(I,IC,IF)
      PCBI(IC,IF)=PCF(IC,IF)-PCP
      PCP=PCF(IC,IF)
802   CONTINUE
801   CONTINUE
C
C INITIAL AND BOUNDARY CONDITIONS FOR CHANNEL BLOCK
      SLOP=0.0
      DO 11 IT=1,ITCOM
      IF(I-2)3,4,5
3       QUP(IT)=QMES(IT,1)
      GO TO 6
4       QUP(IT)=QMES(IT,2)+Q(IT,1)

```

```

      GO TO 6
5      QUP(IT)=Q(IT,2)
6      QLAT(IT)=0.0
      DO 11 IF=1,NFR
      IF(I-2)7,8,9
7      CUP(IT,IF)=GMES(IT,IF,1)/(QUP(IT)*GAMA*SPGR)
      GO TO 10
8      CUP(IT,IF)=(G(IT,1,IF)+GMES(IT,IF,2)/(GAMA*SPGR))/QUP(IT)
      GO TO 10
9      CUP(IT,IF)=G(IT,2,IF)/QUP(IT)
10     GLAT(IT,IF)=0.0
11     CONTINUE
      DO 13 IC=1,INLS
      BEDELV(IC)=BEDLVL(I,IC)
      DO 12 IF=1,NFR
      CI(IC,IF)=CII(I,IC,IF)
      IF(CI(IC,IF).EQ.0.0)CI(IC,IF)=CUP(1,IF)
12     PCBC(IC,IF)=PCKI(IC,IF)
      SLOP=SLOP+SLOPE(IC)
13     CONTINUE
      SLOP=SLOP/FLOAT(INLS)
      QBASE=QUP(1)
      DO 300 IC=1,INL
      QI(IC,1)=QUP(1)
      QI(IC,2)=QUP(1)
      XI(IC)=SLN*FLOAT(IC-1)/FLOAT(INL)
300   KSI(IC)=0
C LIST INITIAL BED ELEVATION AND SIZE COMPOSITION
      WRITE(5,501) I
      WRITE(5,502) (IC,(PCF(IC,IF),IF=1,NFR),BEDELV(IC),IC=1,INLS)
C
C ROUTE WATER AND SEDIMENT THROUGH CHANNEL BLOCK DURING
C CURRENT TIME STEP
      DO 101 IT=1,ITCOM
C
C WATER ROUTING
      CALL WRROUT2
C
C SEDIMENT ROUTING
      CALL SRROUT2
C
      IF(INL.EQ.0) GO TO 129
C RESET INITIAL CONDITIONS FOR FLOW CALCULATIONS
      DO 132 J=1,INL
      XI(J)=XC(J)
      QI(J,1)=QC(J,1)
      QI(J,2)=QC(J,2)
      KSI(J)=KSC(J)
132   CONTINUE
129   CONTINUE
C RESET INITIAL CONDITIONS FOR SEDIMENT CALCULATIONS
      DO 270 IF=1,NFR
      DO 271 IC=1,INLS
      IF(IC.EQ.1) GO TO 272
      CI(IC,IF)=CC(IC,IF)
      GO TO 271
272   CI(IC,IF)=CUP(IT,IF)
271   CONTINUE
270   CONTINUE
      IF(IT.NE.170) GO TO 101

```

```

      WRITE(5,503) IT
      DO 900 IC=1,INLS
      PCF(IC,1)=PCBC(IC,1)
      DO 901 IF=2,NFR
901   PCF(IC,IF)=PCF(IC,IF-1)+PCBC(IC,IF)
900   CONTINUE
C   LIST BED ELEVATION AND SIZE COMPOSITION AT TIME STEP 170
      WRITE(5,502) (IC,(PCF(IC,IF),IF=1,NFR),BEDELV(IC),IC=1,INLS)
101   CONTINUE
C   DISCRETIZED OUTFLOW
      QP=QBASE
      DO 315 IT=1,ITCOM
      QCC=Q(IT,I)
      Q(IT,I)=(QP+QCC)/2.0
      QP=QCC
315   CONTINUE
C
      WRITE(5,504)
      DO 911 IC=1,INLS
      PCF(IC,1)=PCBC(IC,1)
      DO 912 IF=2,NFR
912   PCF(IC,IF)=PCF(IC,IF-1)+PCBC(IC,IF)
911   CONTINUE
C   LIST FINAL BED ELEVATION AND SIZE COMPOSITION
      WRITE(5,502) (IC,(PCF(IC,IF),IF=1,NFR),BEDELV(IC),IC=1,INLS)
C
      DO 913 IC=1,INLS
      BEDLVL(I,IC)=BEDELV(IC)
      DO 914 IF=1,NFR
      PCFF(I,IC,IF)=PCF(IC,IF)
      CII(I,IC,IF)=CI(IC,IF)
914   CONTINUE
913   CONTINUE
201   CONTINUE
C   END OF CHANNEL-BLOCK LOOP
      REWIND 1
C   COMPUTE HYDROGRAPH, SEDIMENTGRAPH, AND SEDIMENT YIELD AT
C   SECTION B-17
      TGOUT=0.0
      TGMES=0.0
      DO 299 IF=1,NFR
      TGO(IF)=0.0
      TGM(IF)=0.0
      TGIN(IF)=0.0
299   CONTINUE
      WRITE(5,505)
      DO 41 IT=1,ITCOM
      QOUT(IT)=Q(IT,NSEG)
      GTOTC(IT)=0.0
      DO 42 IF=1,NFR
      G(IT,NSEG,IF)=G(IT,NSEG,IF)*GAMA*SPPR
      GTOTC(IT)=GTOTC(IT)+G(IT,NSEG,IF)
      TGO(IF)=TGO(IF)+G(IT,NSEG,IF)*DTS
      TGM(IF)=TGM(IF)+GMES(IT,IF,3)*DTS
      TGIN(IF)=TGIN(IF)+(GMES(IT,IF,1)+GMES(IT,IF,2))*DTS
42   CONTINUE
      TGOUT=TGOUT+GTOTC(IT)*DTS
      TGMES=TGMES+GTOTM(IT)*DTS
C   COMPUTE AND LIST CHANGES IN SIZE COMPOSITION OF SEDIMENT
C   LOAD AT B-17 DURING CURRENT TIME BLOCK

```

```

IF(N.NE.1) GO TO 990
IF(IT.EQ.213.OR.IT.EQ.214.OR.IT.EQ.264) GO TO 43
GO TO 41
990 IF(N.NE.2) GO TO 991
IF(IT.EQ.3.OR.IT.EQ.4.OR.IT.EQ.54.OR.IT.EQ.99) GO TO 43
IF(IT.EQ.100.OR.IT.EQ.144.OR.IT.EQ.148.OR.IT.EQ.149) GO TO 43
IF(IT.EQ.189.OR.IT.EQ.191.OR.IT.EQ.193.OR.IT.EQ.239) GO TO 43
IF(IT.EQ.240.OR.IT.EQ.241.OR.IT.EQ.244.OR.IT.EQ.247) GO TO 43
GO TO 41
991 IF(N.NE.3) GO TO 992
IF(IT.EQ.21.OR.IT.EQ.22.OR.IT.EQ.24.OR.IT.EQ.69) GO TO 43
IF(IT.EQ.70.OR.IT.EQ.72.OR.IT.EQ.119.OR.IT.EQ.120) GO TO 43
IF(IT.EQ.165.OR.IT.EQ.167.OR.IT.EQ.212.OR.IT.EQ.213) GO TO 43
IF(IT.EQ.262.OR.IT.EQ.263.OR.IT.EQ.264) GO TO 43
GO TO 41
992 IF(IT.EQ.57.OR.IT.EQ.100.OR.IT.EQ.144.OR.IT.EQ.185) GO TO 43
IF(IT.EQ.186.OR.IT.EQ.192.OR.IT.EQ.237.OR.IT.EQ.238) GO TO 43
GO TO 41
43 CONTINUE
PCW(1)=G(IT,NSEG,1)/GTOTC(IT)*100.0
DO 902 IF=2,NFR
902 PCW(IF)=PCW(IF-1)+G(IT,NSEG,IF)/GTOTC(IT)*100.0
WRITE(S,506) N,IT,(PCW(IF),IF=1,NFR)
41 CONTINUE
C LIST SEDIMENT YIELD, HYDROGRAPH, AND SEDIMENTGRAPH AT B-17
WRITE(S,509) TGMS,TGOUT
WRITE(S,510)
WRITE(S,511) (IF,TGO(IF),TGM(IF),TGIN(IF),IF=1,NFR)
WRITE(S,512)
WRITE(S,513) (I,(QMES(I,J),J=1,3), QDOUT(I),GTOTM(I),GTOTC(I),
&I=1,ITCOM)
999 CONTINUE
C END OF TIME-BLOCK LOOP
C
333 FORMAT(10F7.2)
401 FORMAT(I4)
402 FORMAT(I4,F6.1,F8.3,10F6.2)
403 FORMAT(I4,F10.2)
404 FORMAT(F7.1,F8.5,F7.3,F7.3,3F6.3)
405 FORMAT(10F7.2)
406 FORMAT(14,F7.1,I4,I4)
407 FORMAT(3F7.2,F10.7)
408 FORMAT(10F7.2)
409 FORMAT(4F10.5)
501 FORMAT(//15X,'INITIAL SIZE DISTRIBUTION OF BED MATERIAL AND',
&' BED ELEVATION FOR EACH SECTION OF CHANNEL BLOCK',I4/)
502 FORMAT(15X,I4,10F8.3,F15.7,' FEET')
503 FORMAT(//15X,'SIZE DISTRIBUTION OF BED MATERIAL AND BED ELEVATION',
&' FOR EACH SECTION OF CHANNEL BLOCK AT TIME STEP',I5/)
504 FORMAT(//15X,'FINAL SIZE DISTRIBUTION OF BED MATERIAL AND BED',
&' ELEVATION FOR EACH SECTION OF CHANNEL BLOCK')
505 FORMAT(//15X,'VARIATION OF LOAD SIZE DISTRIBUTION AT B-17 ',
&'DURING CURRENT TIME BLOCK')
506 FORMAT(5X,'TIME BLOCK',I2,3X,'TIME STEP',I4,5X,10F8.3)
509 FORMAT(//15X,'TOTAL MEASURED SEDIMENT YIELD =',F20.5,' LBS.',//15X,
&'TOTAL COMPUTED SEDIMENT YIELD =',F20.5,' LBS.'//)
510 FORMAT(//13X,'SEDIMENT COMPUTED MEASURED',
&,' MEASURED'//13X,'FRACTION YIELD(LBS) YIELD',
&,'(LBS) INFLOW(LBS)'//)
511 FORMAT(15X,I3,F20.5,F20.5,F20.5)

```

```

512 FORMAT(//54X,'MEAS.'/16X,'TIME      COMPUTED FLOW(CFS) AT
&,'FLOW     SED. LOAD(LBS) AT B-17'/16X,'STEP     B-1      B-5M',
&'      B-17    B-17    MEAS.    COMP.'//)
513 FORMAT(15X,I4,6F10.3)
520 FORMAT(2X,F20.5/2X,E15.7)
END FILE 5
STOP
END

C
C          SUBROUTINE WRROUT2
C
C THIS SUBROUTINE ROUTES WATER THROUGH A CHANNEL BLOCK USING THE
C KINEMATIC WAVE SCHEME DEVELOPED BY BORAH ET AL(1980). A LIST OF THE
C IMPORTANT VARIABLES USED IN THIS SUBROUTINE IS GIVEN BELOW:
C
C -----
C          NAME           DESCRIPTION           UNITS
C
C          IC            PARAMETER USED TO LABEL INDIVIDUAL WAVES.      -
C
C          INL           NUMBER OF NODE POINTS IN THE CHANNEL BLOCK       -
C
C          IS             COUNTS NUMBER OF SHOCK WAVES OCCURRING AT THE END      -
C                      OF THE CURRENT TIME STEP.
C
C          KSC(IC)        FLAG USED TO CHARACTERIZE THE WAVE IC OCCURRING IN      -
C                      THE CHANNEL BLOCK, AT THE END OF THE CURRENT TIME      -
C                      STEP. KSC=0 FOR CHARACTERISTICS, KSC>0 FOR SHOCKS.
C
C          KSI(IC)        FLAG USED TO CHARACTERIZE THE WAVE IC OCCURRING IN      -
C                      THE CHANNEL BLOCK, AT THE START OF THE CURRENT TIME      -
C                      STEP. KSI=0 FOR CHARACTERISTICS, KSI>0 FOR SHOCKS.
C
C          Q(IT,I)        COMPUTED WATER OUTFLOW FROM THE CHANNEL BLOCK I, AT CFS
C                      THE END OF THE CURRENT TIME STEP IT.
C
C          QC(IC,L)       FLOW DISCHARGE AHEAD (L=1) OR BEHIND (L=2) OF THE      CFS
C                      SHOCK IC, AT THE END OF THE CURRENT TIME STEP.
C
C          QI(IC,L)       FLOW DISCHARGE AHEAD (L=1) OR BEHIND (L=2) OF THE      CFS
C                      SHOCK IC, AT THE START OF THE CURRENT TIME STEP.
C
C          XC(IC)         DISTANCE OF WAVE FRONT IC TO UPSTREAM END OF THE      FT
C                      CHANNEL BLOCK, AT THE END OF THE CURRENT TIME STEP.
C
C          XI(IC)         DISTANCE OF WAVE FRONT IC TO UPSTREAM END OF THE      FT
C                      CHANNEL BLOCK, AT THE START OF THE CURRENT TIME STEP.
C
C -----
C
C          COMMON /ROUT/ I,IT,SLN,CHEZY,DTS,ITCOM,INL,QBASE,
&QUP(300),QI(50,2),XI(50),KSI(50),Q(300,3)
COMMON /WRROUT/ SLOP,QLAT(300),QC(50,2),XC(50),KSC(50)
EXP=1.5
BET=1.0/EXP
EXP1=EXP+1.0
EXM1=EXP-1.0
KIN=CHEZY*SLOP**0.5
TERM=EXP*KIN*DTS
QL=QLAT(IT)
QU=QUP(IT)

```

```

      IF(QL.EQ.0.0 AND QU.EQ.0.0) GO TO 130
C PROJECT ALL CHARACTERISTICS TO NEW TIME LEVEL
      AC=(QU/KIN)**RET+QL*DTS/2.0
      QC(1,1)=KIN*AC**EXP
      IF(QL.EQ.0.0) GO TO 102
      XC(1)=(QC(1,1)-QU)/QL
      GO TO 103
102  XC(1)=TERM*AC**EXM1/2.0
103  ICST=1
      KSC(1)=0
      GO TO 131
130  ICST=0
131  IF(INL.EQ.0) GO TO 150
      IS=0
      DO 104 IC=1,INL
      IA=IC+ICST-IS
      IF(KSI(IC).EQ.0.OR.QI(IC,1).GE.QI(IC,2)) GO TO 105
C PROPAGATION OF SHOCK WAVE
      AA=(QI(IC,1)/KIN)**BET
      AB=(QI(IC,2)/KIN)**BET
      AAF=AA+QL*DTS
      ABF=AB+QL*DTS
      QC(IA,1)=KIN*AAF**EXP
      QC(IA,2)=KIN*ABF**EXP
      IF(QL.EQ.0.0) GO TO 108
      PROD=ALP/(EXP1*(AB-AA)*QL)
      XC(IA)=XI(IC)+PROD*(ABF**EXP1-AAF**EXP1-AB**EXP1+AA**EXP1)
      GO TO 107
108  XC(IA)=XI(IC)+(QI(IC,2)-QI(IC,1))*DTS/(AB-AA)
      GO TO 107
C PROPAGATION OF CHARACTERISTIC WAVE
105  KSI(IC)=0
      AC=(QI(IC,1)/KIN)**RET+QL*DTS
      QC(IA,1)=KIN*AC**EXP
      IF(QL.EQ.0.0) GO TO 106
      XC(IA)=XI(IC)+(QC(IA,1)-QI(IC,1))/QL
      GO TO 107
106  XC(IA)=XI(IC)+TERM*AC**EXM1
C CHECK FOR NEW SHOCK FORMATION
107  IF(KSI(IC).GT.0) GO TO 109
      IF(IA.EQ.1) GO TO 140
      IF(XC(IA).LE.XC(IA-1)) GO TO 110
C NO SHOCK IS FORMED
140  KSC(IA)=0
      GO TO 104
C SHOCK IS FORMED
110  IA=IA-1
      IF(KSC(IA).GT.0) GO TO 112
C SHOCK IS FORMED BY TWO CHARACTERISTIC WAVES
      XC(IA)=(XC(IA)+XC(IA+1))/2.0
      QC(IA,1)=QC(IA+1,1)
      QC(IA,2)=QC(IA,1)
      IS=IS+1
      KSC(IA)=1
      GO TO 104
C THE CHARACTERISTIC WAVE JOINS THE SHOCK AHEAD OF THE FRONT
112  XC(IA)=XC(IA)
      QC(IA,1)=QC(IA+1,1)
      IS=IS+1
      KSC(IA)=11

```

```

      GO TO 104
C  CHECK IF THE PROPAGATING SHOCK IS INTERSECTED BY ANY OTHER SHOCK
C  OR CHARACTERISTIC WAVE
109  IF(IA.EQ.1) GO TO 141
     IF(XC(IA).LE.XC(IA-1)) GO TO 113
C  THE PROPAGATING SHOCK IS NOT INTERSECTED
141  KSC(IA)=1
     GO TO 104
C  THE PROPAGATING SHOCK IS INTERSECTED
113  IA=IA-1
     IF(KSC(IA).GT.0) GO TO 114
C  THE PROPAGATING SHOCK IS JOINED BY A CHARACTERISTIC WAVE
C  BEHIND THE FRONT
     XC(IA)=XC(IA+1)
     QC(IA,2)=QC(IA,1)
     QC(IA,1)=QC(IA+1,1)
     IS=IS+1
     KSC(IA)=11
     GO TO 104
C  NEW SHOCK IS FORMED BY TWO INTERSECTING SHOCKS
114  XC(IA)=(XC(IA)+XC(IA+1))/2.0
     QC(IA,1)=QC(IA+1,1)
     QC(IA,2)=QC(IA,2)
     IS=IS+1
     KSC(IA)=2
104  CONTINUE
C  COMPUTE OUTFLOW FROM CHANNEL BLOCK DURING CURRENT TIME STEP
150  CONTINUE
     IAD=0
     IF(INL.EQ.0) IA=ICST
     IF(IA.EQ.0) GO TO 122
     XB=0.0
     QB=QU
     DO 115 J=1,IA
     IF(XC(IA).GE.SLN) GO TO 117
     XB=XC(IA)
     QB=QC(IA,1)
     IF(KSC(IA).GT.0) QB=(QC(IA,1)+QC(IA,2))/2.0
117  IC=IA-J+1
     IF(XC(IC).LT.SLN) GO TO 115
     IAD=IAD+1
     XA=XC(IC)
     QA=QC(IC,1)
     IF(KSC(IC).GT.0) QA=(QC(IC,1)+QC(IC,2))/2.0
115  CONTINUE
     IF(IAD.GT.0) GO TO 118
     AI=(QBASE/KIN)**BET
     IF(IT.GT.1) AI=(Q(IT-1,I)/KIN)**BET
     AC=AI+QL*DTS
     QA=KIN*AC**EXP
     XA=TERM*AC**EXM1+SLN
     IF(QL.GT.0.0) XA=(QA-Q(IT-1,I))/QL+SLN
118  Q(IT,I)=QB+(QA-QB)*(SLN-XB)/(XA-XB)
     INL=IA-IAD
     GO TO 123
122  Q(IT,I)=0.0
     INL=0
123  RETURN
     END
C

```

```

        SUBROUTINE SRROUT2
C
C THIS SUBROUTINE PERFORMS SEDIMENT CALCULATIONS AT ALL NODE POINTS
C IN THE CHANNEL BLOCK DURING CURRENT TIME STEP
C
      DIMENSION WATMAT(10),BEDMAT(10),SCAP(10),ERS(10),ACCM(10,10),
     &TCA(10)
      COMMON /ROUT/ I,IT,SIN,CHEZY,DTS,ITCOM,INL,QBASE,
     &QUP(300),QI(50,2),XI(50),KSI(50),Q(300,3)
      COMMON /SRROUT/ SPGR,CAMA,SNU,NFR,INLS,WIDTH(10),SLOPE(10),
     &CPER(10),EPR(10),CDEP(10),EDEP(10),GLAT(300,10),XSI(10),
     &XSC(10,10),BEDELV(10),CI(10,10),CC(10,10),PCBI(10,10),PCRC(10,10),
     &CUP(300,10),DMM(10),COEF(10),VS(10),POR(10),G(264,3,10),PCW(10),
     &ERO,CHI,CEL
C
      DO 204 IC=1,INLS
C
C INTERPOLATE FLOW VALUES AT THE NODE POINTS
      IF(IC.EQ.1) GO TO 205
      IF(XSI(IC).LT.XI(1)) GO TO 206
      DO 207 J=1,100
      IF(XSI(IC).GE.XI(J).AND.XSI(IC).LT.XI(J+1)) GO TO 208
      GO TO 207
208  Q1=QI(J,1)
      IF(KSI(J).GT.0) Q1=(QI(J,1)+QI(J,2))/2.0
      Q2=QI(J+1,1)
      IF(KSI(J+1).GT.0) Q2=(QI(J+1,1)+QI(J+2,2))/2.0
      QP=Q1+(Q2-Q1)*(XSI(IC)-XI(J))/(XI(J+1)-XI(J))
      GO TO 209
207  CONTINUE
      GO TO 209
206  IF(IT.EQ.1) GO TO 210
      Q1=QUP(IT-1)
      GO TO 211
210  Q1=QI(IC,1)
211  Q2=QI(1,1)
      IF(KSI(1).GT.0) Q2=(QI(1,1)+QI(1,2))/2.0
      QP=Q1+(Q2-Q1)*XSI(IC)/XI(1)
      GO TO 209
205  IF(IT.EQ.1) GO TO 212
      QP=QUP(IT-1)
      GO TO 209
212  QP=QI(IC,1)
209  CONTINUE
C
C UPDATE THE HYDRAULIC PARAMETERS AT THE NODE POINTS
      SLP=SLOPE(IC)
      WDTH=WIDTH(IC)
      CPR=CPER(IC)
      EPR=EPR(IC)
      CDP=CDEP(IC)
      EDP=EDEP(IC)
      EXP=1.5
      BET=1.0/EXP
      KIN=CHEZY*SLP**0.5
      QE=QP
      AE=(QE/KIN)**BET
      IF(AE.LT.1.0E-5) GO TO 213
      VEL=QE/AE
      DPTH=CDP*AE**EDP

```

```

WEP=CPR*AE**EPR
RHB=AE/WEP
HYR=DPTH
UST=SQRT(32.2*HYR*SLP)
IF(IC.EQ.INLS) GO TO 241
DELX=XSI(IC+1)-XSI(IC)
GO TO 242
241 DELX=SLN-XSI(INLS)
242 CONTINUE
C
C COMPUTE TRANSPORT CAPACITIES AND TERM DELTA (EQ. 11)
SUM=0.0
DO 220 IF=1,NFR
GL=GLAT(IT,IF)
CP=CI(IC,IF)
D=DMM(IF)
DFT=DMM(IF)/304.8
W=VS(IF)
IF(DMM(IF).LE.4.0) GO TO 860
IF(DMM(IF).LT.5.0) GO TO 861
MEYERP=8.0
CALL MEYER(MEYERP,UST,RHB,DFT,GAMA,SNU,SPGR,WDTH,QE,VEL,CONC)
SCAP(IF)=CONC*AE/1.0E6/SPGR
IF(DMM(IF).GT.30.0) SCAP(IF)=0.0
GO TO 862
860 CALL YANG(DFT,UST,SNU,VEL,SLP,W,SPGR,CONC)
SCAP(IF)=CONC*AE/1.0E6/SPGR
GO TO 862
861 CALL DUBOYS(D,DFT,AE,WDTH,SLP,SPGR,SNU,GAMA,CHI,UST,SFLOW)
SCAP(IF)=SFLOW/VEL
862 WATMAT(IF)=CP*AE+GL*DELX/VEL
IF(SCAP(IF).EQ.0.0) GO TO 220
SUM=SUM+WATMAT(IF)/SCAP(IF)
220 CONTINUE
C
C COMPUTE ACTIVE (OR ARMOR) LAYER THICKNESS
PARM=0.0
NARM=NFR
DARM=DMM(NFR)
DO 810 IF=1,NFR
IF(SCAP(IF).GT.0.0) GO TO 810
IF(IF.EQ.1) GO TO 811
IF(SCAP(IF-1).GT.0.0) GO TO 811
GO TO 812
811 NARM=IF
DARM=DMM(IF)
812 PARM=PARM+PCBC(IC,IF)
810 CONTINUE
IF(PARM.LT.0.0) GO TO 814
DO 815 IFF=1,NFR
IFA=NFR-IFF+1
NARM=IFA
DARM=DMM(IFA)
PARM=PCBC(IC,IFA)
IF(PARM.LT.0.0) GO TO 814
815 CONTINUE
814 ARMHT=100.0*DARM/PARM/304.8
C COMPUTE VOLUME OF BED MATERIAL FRACTIONS IN ACTIVE LAYER
DO 813 IF=1,NFR
813 BEDMAT(IF)=ARMHT*PCBC(IC,IF)*WDTH/100.0

```

```

        IF(1.0-SUM) 222,223,224
222  CONTINUE
C
C   DEPOSITION LOOP
    TBM=0.0
    BEDUP=0.0
    DO 230 J=1,NFR
    IF=NFR-J+1
    CP=CI(IC,IF)
    IF(SCAP(IF).EQ.0.0) GO TO 231
    RESCAP=SCAP(IF)*(1.0-SUM)
    DEPO=0.0
    IF(RESCAP.GE.0.0) GO TO 232
    IF(ABS(RESCAP).GT.WATMAT(IF)) GO TO 231
    DEPO=ABS(RESCAP)
    GO TO 232
231  DEPO=WATMAT(IF)
232  BT=2.0*VS(IF)*DTS/RHE
    IF(BT.LT.1.0)DEPO=BT*DEPO
    WATMAT(IF)=WATMAT(IF)-DEPO
    ADD=0.0
    IF(SCAP(IF).GT.0.0) ADD=DEPO/SCAP(IF)
    SUM=SUM+ADD
C   UPDATE LOAD AT NODE POINTS
    CAP=SCAP(IF)/AE
    CCC=WATMAT(IF)/AE
    XKP=CAP-0.999*CP
    XKC=CAP-0.999*CCC
    ADD=0.0
    IF(CAP.GT.0.0) ADD=CLL*CAP/(AE*XKP*XKC)
    IF(ADD.LT.0.0) ADD=0.0
    FNLR=1.0+ADD
    DELT=DELX*FNLR/VEL
    IF(DELT.LT.DTS) GO TO 2200
    IF(IC.EQ.INLS) GO TO 233
    CCI=CI(IC+1,IF)
    CCI(IF)=CCI+(CCC-CCI)*DTS/DELT
    GO TO 234
C   SEDIMENT OUTFLOW FROM CHANNEL BLOCK
233  IF(IT.EQ.1) GO TO 235
    CCI=G(IT-1,I,IF)/Q(IT-1,I)
    GO TO 236
235  CCI=CI(IC,IF)
236  G(IT,I,IF)=(CCI+(CCC-CCI)*DTS/DELT)*Q(IT,I)
    GO TO 234
2200 XDEL=DELT*VEL/FNLR
    IF(IC.EQ.1) GO TO 2201
    CCI=CC(IC,IF)
    GO TO 2202
2201 CCB=CUP(IT,IF)
2202 CC(IC+1,IF)=CCB+(CCC-CCR)*DELX/XDEL
    IF(IC.EQ.INLS) G(IT,I,IF)=CC(IC+1,IF)*Q(IT,I)
234  BEDMAT(IF)=BEDMAT(IF)+DEPO*DTS/DELT
    TRM=TRM+BEDMAT(IF)
    BEDUP=BEDUP+DEPO*DTS/DELT/WDTH/POR(IF)
230  CONTINUE
C   CHANGE IN BED ELEVATION AND BED LAYER COMPOSITION
    BEDELV(IC)=BEDELV(IC)+BEDUP
    DO 239 IF=1,NFR
239  PCBC(IC,IF)=BEDMAT(IF)/TRM*100.0

```

```

        GO TO 204
223    CONTINUE
C
C   EQUILIBRIUM LOOP
    DO 240 IF=1,NFR
    CP=CI(IC,IF)
    CCC=WATMAT(IF)/AE
    CAP=SCAP(IF)/AE
    XKP=CAP-0.999*CP
    XKC=CAP-0.999*CCC
    ADD=0.0
    IF(CAP.GT.0.0) ADD=CEL*CAP/(AE*XKP*XKC)
    IF(ADD.LT.0.0) ADD=0.0
    FNLR=1.0+ADD
    DELT=DELX*FNLR/VEL
C   UPDATE LOAD AT NODE POINTS
    IF(DELT.LT.DTS) GO TO 2300
    IF(IC.EQ.INLS) GO TO 243
    CCI=CI(IC+1,IF)
    CC(IC+1,IF)=CCI+(CCC-CCI)*DTS/DELT
    GO TO 240
C   SEDIMENT OUTFLOW FROM CHANNEL BLOCK
243    IF(IT.EQ.1) GO TO 244
    CCI=G(IT-1,I,IF)/Q(IT-1,I)
    GO TO 245
244    CCI=CI(IC,IF)
245    G(IT,I,IF)=(CCI+(CCC-CCI)*DTS/DELT)*Q(IT,I)
    GO TO 240
2300  XDEL=DELT*VEL/FNLR
    IF(IC.EQ.1) GO TO 2301
    CCB=CC(IC,IF)
    GO TO 2302
2301  CCB=CUP(IT,IF)
2302  CC(IC+1,IF)=CCB+(CCC-CCB)*DELX/XDEL
    IF(IC.EQ.INLS) G(IT,I,IF)=CC(IC+1,IF)*Q(IT,I)
240    CONTINUE
    GO TO 204
224    CONTINUE
C
C   EROSION AND ARMORING CALCULATIONS
C
C   COMPUTE VOLUME ENTRAINMENT MATRIX
    DO 281 IFA=1,NFR
    DEN=0.0
    LOOP=NFR-IFA+1
    DO 282 J=1,LOOP
    IF=J+IFA-1
282    DEN=DFN+COEF(J)*BEDMAT(IF)
    DO 283 J=1,LOOP
    IF=J+IFA-1
    IF(DEN.EQ.0.0) GO TO 830
    ACCM(IF,IFA)=COEF(J)*BEDMAT(IF)/DEN*BEDMAT(IF)
    GO TO 283
830    ACCM(IF,IFA)=0.0
283    CONTINUE
281    CONTINUE
C
C   EROSION LOOP
    DO 278 IF=1,NFR
    TCA(IF)=0.0

```

```

DO 279 IFA=1,IF
279   TCA(IF)=TCA(IF)+ACCM(IF,IFA)
CONTINUE
DO 237 IF=1,NFR
237   ERS(IF)=0.0
DO 284 IF=1,NFR
IF(SCAP(IF).EQ.0.0) GO TO 284
RESCAP=SCAP(IF)*(1.0-SUM)
IF(RESCAP.LE.0.0) GO TO 285
IF(RESCAP.GE.TCA(IF)) GO TO 286
DO 831 J=1,IF
DO 287 J1=1,IF
IF(J1.EQ.1) IFA=IF
IF(J1.GT.1) IFA=J1-1
IF(SCAP(IFA).EQ.0.0) GO TO 287
RESCAP=SCAP(IFA)*(1.0-SUM)
CNTBN=ACCM(IF,IFA)/FLOAT(IF)
IF(RESCAP.GT.CNTBN) GO TO 288
EROSN=ERO*RESCAP
GO TO 289
288   EROSN=ERO*CNTBN
289   ERS(IFA)=ERS(IFA)+EROSN
SUM=SUM+EROSN/SCAP(IFA)
IF(SUM.GE.1.0) GO TO 285
287   CONTINUE
831   CONTINUE
286   CONTINUE
DO 290 IFA=1,IF
IF(SCAP(IFA).EQ.0.0) GO TO 290
EROSN=ERO*ACCM(IF,IFA)
ERS(IFA)=ERS(IFA)+EROSN
SUM=SUM+EROSN/SCAP(IFA)
290   CONTINUE
284   CONTINUE
C UPDATE LOAD AT NODE POINTS
285   CONTINUE
TRM=0.0
BEDWN=0.0
DO 250 IF=1,NFR
CP=CI(IC,IF)
WATMAT(IF)=WATMAT(IF)+ERS(IF)
CCC=WATMAT(IF)/AE
CAP=SCAP(IF)/AE
XKP=CAP-0.999*CP
XKC=CAP-0.999*CCC
ADD=0.0
IF(CAP.GT.0.0) ADD=CP*(CAP/(AE*XKP*XKC))
IF(ADD.LT.0.0) ADD=0.0
FNLR=1.0+ADD
DELT=DELX*FNLR/VEL
IF(DELT.LT.DTS) GO TO 2400
IF(IC.EQ.JNLS) GO TO 251
CCI=CI(IC+1,IF)
CCI(IF)=CCI+(CCC-CCI)*DTS/DELT
GO TO 252
C SEDIMENT OUTFLOW FROM CHANNEL BLOCK
251   IF(IT.EQ.1) GO TO 253
CCI=G(IT-1,I,IF)/Q(IT-1,I)
GO TO 254
253   CCI=CI(IC,IF)

```

```

254 G(IT,I,IF)=(CCI+(CCC-CCI)*DTS/DELT)*Q(IT,I)
GO TO 252
2400 XDEL=DELT*VEL/FNLR
IF(IC.EQ.1) GO TO 2401
CCB=CC(IC,IF)
GO TO 2402
2401 CCB=CUP(IT,IF)
2402 CC(IC+1,IF)=CCB+(CCC-CCB)*DELX/XDEL
IF(IC.EQ.INLS) G(IT,I,IF)=CC(IC+1,IF)*Q(IT,I)
252 TERS=ERS(IF)*DTS/DELT
IF(TERO.GT.BEDMAT(IF)) TER0=BEDMAT(IF)
BEDMAT(IF)=BEDMAT(IF)-TERO
TBM=TBM+BEDMAT(IF)
C UPDATE BED ELEVATION
BEDWN=BEDWN+TERO/WDTH/POR(IF)
250 CONTINUE
BEDELV(IC)=BEDELV(IC)-BEDWN
C ADJUSTMENT OF ACTIVE LAYER THICKNESS
IF(TBM GT 0.0) GO TO 294
DO 293 IF=1,NFR
293 PCBC(IC,IF)=PCBI(IC,IF)
GO TO 204
294 CONTINUE
PARM=0
DO 295 IF=1,NFR
PCBC(IC,IF)=BEDMAT(IF)/TBM*100.0
IF(SCAP(IF) GT 0.0) GO TO 295
PARM=PARM+PCBC(IC,IF)
295 CONTINUE
IF(PARM LT 0.0) GO TO 820
DO B21 IFF=1,NFR
IFA=NFR-IFF+1
NARM=IFA
DARM=DMM(IF)
PARM=PCBC(IC,IFA)
IF(PARM GT 0.0) GO TO 820
821 CONTINUE
820 CURARM=100.0/PARM*DARM/304.8
ADHT=CURARM-TBM/WDTH
IF(ADHT LT 0.0) GO TO 204
ADARM=ADHT
TBM=0
DO 296 IF=1,NFR
BEDMAT(IF)=BEDMAT(IF)+ADARM*PCBI(IC,IF)/100.0*WDTH
296 TBM=TBM+BEDMAT(IF)
DO 297 IF=1,NFR
297 PCBC(IC,IF)=BEDMAT(IF)/TBM*100.0
GO TO 204
213 CONTINUE
C DEPOSITION CAUSED BY TERMINATION OF FLOW
DO 260 IF=1,NFR
IF(IC.EQ.INLS) GO TO 261
CC(IC+1,IF)=0.0
GO TO 262
261 G(IT,I,IF)=0.0
262 BEDMAT(IF)=BEDMAT(IF)+CI(IC,IF)*AE
260 CONTINUE
204 CONTINUE
RETURN
END

```

```

C
C      SUBROUTINE DUBOYS(D,DFT,AE,WDTH,SLP,SPCR,SNU,GAMA,CHI,
C      &UST,SFLOW)
C
C      THIS SUBROUTINE COMPUTES THE TRANSPORT RATE OF NONCOHESIVE
C      SEDIMENTS USING A DUBOYS TYPE FORMULA(GRAF, 1971)
C
C          CALL SHIELD(DFT,SPCR,SNU,GAMA,UST,TC)
C          CHI=CHI/(D**0.75)
C          TAO=GAMA*AE/WDTH*SLP
C          SFLOW=WDTH*CHI*TAO*(TAO-TC)
C          IF(SFLOW.LE.0.0) SFLOW=0.0
C          RETURN
C          END
C
C          SUBROUTINE MEYER(MEYERP,USTAR,RHH,D,WEIGHT,VTSC,S,WIDTH,Q,V,GR,X0)
C
C          THIS SUBROUTINE COMPUTES THE TRANSPORT RATE OF NONCOHESIVE
C          SEDIMENTS USING THE BEDLOAD FORMULA DEVELOPED BY MEYER-PETER
C          AND MULLER(1948)
C
C          FCTN(F,RO,REY)=(1./SQRT(F))-2.* ALOG10(RO)-1.14+2.*ALOG10(1.+9.35*
C          *RO/(REY*SQRT(F)))
C          G=32.17
C          REY=4.0*RHH*V/VISC
C          RO=2.*RHH/D
C          RSTAR=2.*D*USTAR/VISC
C          IF(RSTAR.GT.70.0) GO TO 7
C
C          F1=0.006
C          F2=0.09
C          I=0
C          FCT1=FCTN(F1,RO,REY)
C          F3=0.5*(F1+F2)
C          FCT3=FCTN(F3,RO,REY)
C          IF(FCT1*FCT3).GT.1.5,2
C          1      F2=F3
C          GO TO 3
C          2      F1=F3
C          3      IF(ABS(F2-F1).LT.0.0001)5,5,4
C          4      I=I+1
C          IF(I.LT.100) GO TO 6
C          GO TO 7
C          5      F=F3
C          GO TO 8
C          7      F=(1.0/(2.*ALOG10(RO)+1.14))**2.
C          8      AK=V*SQRT(F/8.)/USTAR
C          AK=0.75
C
C          Y=(USTAR*USTAR)/((S-1.0)*G*D)
C          G1=MEYERP*WIDTH*(USTAR**3.0)*(WEIGHT/G)*(S/(S-1.0))
C          CALL SHIELD(D,S,VISC,WEIGHT,USTAR,TC)
C          TSTAR=TC/((S-1.0)*WEIGHT*D)
C          TSTAR=0.047
C          G2=AK**1.5-(TSTAR/Y)
C          IF(G2.LT.0.0) GO TO 9
C          G2=G2**1.5
C          GR=G1*G2
C          X0=(GR*1.0E6)/(Q*WEIGHT)
C          GO TO 10

```

```

9      GB=0.0
10     XD=0.0
11     RETURN
12     END
C
C      SUBROUTINE YANG(DFT,UST,SNU,V,SLP,W,S,CONC)
C
C      THIS SUBROUTINE COMPUTES THE TRANSPORT RATE OF NONCOHESIVE SEDIMENTS
C      USING THE TOTAL LOAD FORMULA DEVELOPED BY YANG(1973)
C
13     D=DFT
14     A=UST*D/SNU
15     IF(A.LE.70.0) GO TO 7
16     VCW=2.5/( ALOG10(A)-0.06)+0.66
17     GO TO 8
18     VCW=2.05
19     ESP=V*SLP/W-VCW*SLP
20     IF(ESP) 9,9,10
21     CONC=0.0
22     GO TO 11
23     F1=5.435-0.286*ALOG10(U*D/SNU)-0.457*ALOG10(UST/W)
24     F2=1.799-0.409*ALOG10(W*D/SNU)-0.314*ALOG10(UST/W)
25     F3=ALOG10(ESP)
26     E=F1+F2*F3
27     C=10.0**E
28     CONC=C
29     CONTINUE
30     RETURN
31     END
C
C      SUBROUTINE SHIELD(D,S,VISC,WEIGHT,USTAR,TC)
C
C      THIS SUBROUTINE COMPUTES THE CRITICAL BED SHEAR STRESS DERIVED
C      FROM SHIELDS' FUNCTION
32     REY=USTAR*D/VISC
33     IF(REY.GT.10.0) GO TO 1
34     TC=0.08*(S-1.0)*WEIGHT*D/REY**0.4
35     GO TO 3
36     IF(REY.GT.500.0) GO TO 2
37     TC=0.022*(S-1.0)*WEIGHT*D*REY**0.16
38     GO TO 3
39     TC=0.06*(S-1.0)*WEIGHT*D
40     CONTINUE
41     RETURN
42     END
C
C      SUBROUTINE SETVEL(D,W)
C
C      THIS SUBROUTINE COMPUTES THE SETTLING VELOCITY OF SEDIMENT PARTICLES
43
44     DIMENSION A(2,11)
45     DATA A(1,1),A(1,2),A(1,3),A(1,4),A(1,5),A(1,6),A(1,7),A(1,8),
46     &A(1,9),A(1,10),A(1,11)/
47     &0.04,0.06,0.10,0.20,0.40,0.80,1.50,2.00,3.00,7.00,10.00/
48     DATA A(2,1),A(2,2),A(2,3),A(2,4),A(2,5),A(2,6),A(2,7),A(2,8),
49     &A(2,9),A(2,10),A(2,11)/
50     &0.14,0.32,0.76,2.20,5.30,10.50,16.90,20.30,25.60,39.50,44.00/
51     IF(D.LE.0.04) GO TO 20
52     IF(D.GE.10.0) GO TO 21
53     GO TO 22
54     W=0.14/0.04*D

```

```
      GO TO 100
21   W=4.5/3.0*(D-10.0)+44.0
      GO TO 100
22   CONTINUE
      DO 10 I=1,11
      IF(A(1,I).GT.D) GO TO 11
      D1=A(1,I)
      W1=A(2,I)
      GO TO 10
11   D2=A(1,I)
      W2=A(2,I)
      GO TO 12
10   CONTINUE
12   W=(W2-W1)*(D-D1)/(D2-D1)+W1
100  RETURN
      END
```